

# Fixation and extinction in time-fluctuating spatially structured metapopulations

Matthew Asker,<sup>1,\*</sup> Mohamed Swailem,<sup>2</sup> Uwe C. Täuber,<sup>2</sup> and Mauro Mobilia<sup>1,†</sup>

<sup>1</sup>*Department of Applied Mathematics, School of Mathematics,  
University of Leeds, Leeds LS2 9JT, United Kingdom*

<sup>2</sup>*Department of Physics & Center for Soft Matter and Biological Physics,  
MC 0435, Robeson Hall, 850 West Campus Drive,  
Virginia Tech, Blacksburg, Virginia 24061, USA*

(Dated: April 14, 2025)

Bacteria evolve in volatile environments and complex spatial structures. Migration, fluctuations and environmental variability therefore have a significant impact on the evolution of microbial populations. Here, we consider a class of spatially explicit metapopulation models arranged as regular (circulation) graphs where wild-type and mutant cells compete in a *time-fluctuating* environment where demes (subpopulations) are connected by slow cell migration. The carrying capacity is the same at each deme and endlessly switches between two values associated to harsh and mild environmental conditions. When the rate of switching is neither too slow nor too fast, the dynamics is characterised by bottlenecks and the population is prone to fluctuations or extinction. We analyse how slow migration, spatial structure, and fluctuations affect the phenomena of fixation and extinction on clique, cycle, and square lattice metapopulations. When the carrying capacity remains large, bottlenecks are weak and deme extinction can be ignored. The dynamics is thus captured by a coarse-grained description within which the probability and mean time of fixation are obtained analytically. This allows us to show that, in contrast to what happens in static environments, the mutant fixation probability depends on the rate of migration. We also show that the fixation probability and mean fixation time can exhibit a non-monotonic dependence on the switching rate. When the carrying capacity is small under harsh conditions, bottlenecks are strong, and the metapopulation evolution is shaped by the coupling of deme extinction and strain competition. This yields rich dynamical scenarios, among which we identify the best conditions to eradicate mutants without dooming the metapopulation to extinction. We offer an interpretation of these findings in the context of an idealised treatment and discuss possible generalisations of our models.

## I. INTRODUCTION

Microbial populations live in volatile and time-varying environments embedded in complex spatial settings, across which the distribution of microbes fluctuates. For instance, many organisms live in densely packed aggregates on surface-attached biofilms [1], numerous commensal bacteria are distributed throughout the gastrointestinal tract [2, 3], and patients' organs are spatial environments between which bacteria can migrate [4]. Moreover, natural environments are not static, e.g. temperature, pH, or available resources change over time. These abiotic variations, not caused by the organisms themselves, are referred to as environmental fluctuations and can have a significant influence on the evolution of natural populations. For example, the gut microbiome of a host is exposed to fluctuations of great amplitude on various timescales, and these affect the diversity of the microbiota [5, 6]. In small populations, demographic fluctuations are another important form of randomness resulting in fixation - where one strain takes over the community - or extinction [7, 8]. Since the variations of population size and composition are often interdependent [9–15], this can

lead to the coupling of environmental and demographic fluctuations [16–24]. Their interplay is particularly significant in microbial communities, where it can lead to population bottlenecks, where new colonies consisting of a few cells are prone to fluctuations [25–29]. Population bottlenecks and fluctuations are particularly relevant for the evolution of antimicrobial resistance, when cells surviving antibiotics treatment may replicate leading to the spread of resistance [21, 24, 30–32].

How likely is a population to be taken over by a mutant or to go extinct? What is the typical time for these events to occur? These are central questions in evolution, and the answers depend on the population's spatial structure as well as the environmental variations and fluctuations. In this context, it is important to understand the impact of spatial structure, migration, and fluctuations on the spread of a mutant strain. A common approach to represent a spatially structured biological population is by dividing it into several demes - well-mixed subpopulations connected by cell migration - hence forming a *metapopulation* [33–42]. The influence of the spatial arrangement of a population and stochastic fluctuations on mutants' fate has been studied in *static* environments both theoretically [33, 34, 41, 43–54] and experimentally [55–58]. Maruyama notably showed that in a constant environment, when cell migration is symmetric and preserves the overall mutant fraction, the fixation probability of a mutant is independent of the spatial structure and migra-

\* mmmwa@leeds.ac.uk

† M.Mobilia@leeds.ac.uk

‡ <https://eedfp.com>

tion rate [43]. However, it has been shown that random extinction and recolonisation can affect the mutant fixation probability on fully-connected (static) graphs, even when cell migration is symmetric [44]. In this case, deme extinction is immediately followed by recolonisation by a mixture of cells from other demes [35, 36, 44]. Furthermore, independent extinction and recolonisation by a single neighbour of demes has been studied on fully-connected (static) graphs [59]. Recently, the authors of Ref. [41] studied the influence of slow migration on the fate of mutants on static graphs, and demonstrated that migration asymmetry can dramatically affect their fixation probability on certain spatial structures like the star graph. However, the biologically relevant problem of mutants evolving in time-varying spatially structured populations has been rather scarcely investigated, and the case of strains competing to colonise and fixate demes prone to extinction remains under-explored.

Here, we tackle these important issues by studying a class of time-fluctuating microbial metapopulation models consisting of demes in which wild-type and mutant cells evolve in a time-varying environment represented by a switching carrying capacity. We use coarse-grained descriptions of the dynamics to study the joint influence of environmental variability, demographic fluctuations, migration, and spatial structure on the evolution of the metapopulation. We obtain explicit results for cliques (island model [33, 34], or fully-connected graph), cycles, and two-dimensional grids (with periodic boundaries). In stark contrast with the evolution in static environments, we demonstrate that when bottlenecks are weak, the fixation probability on regular circulation graphs depends on the migration rate. Moreover, we show that under the effect of environmental variability and fluctuations the fixation probability and mean fixation time can exhibit a non-monotonic dependence on the switching rate. In the case of strong bottlenecks, arising when the carrying capacity is small under harsh conditions, the dynamics is characterised by deme extinction and strain competition coupled by environmental switching. This yields rich dynamical scenarios among which we identify the best conditions to eradicate mutants without risking metapopulation extinction.

In the next section, we introduce the explicit spatial metapopulation model that we study and outline our methodology. In Sec. III, we present our results in the case of static environments. This paves the way to the detailed analysis in time-fluctuating environments of Sec. IV, with the weak and strong bottleneck regimes respectively studied in Secs. IV 1 and IV 2. Sec. V is dedicated to a discussion of our findings, assumptions and possible generalisations. We present our conclusions in Sec. VI. Additional technical details are given in a series of appendices.

## II. MODEL & METHODS

We consider a class of spatially explicit metapopulation models of  $\Omega$  demes labelled by  $x \in \{1, \dots, \Omega\}$ , each of which at time  $t$  consists of a well-mixed subpopulation of  $n_W$  cells of wild-type  $W$ , and  $n_M$  mutants of strain  $M$ . Wild-type cells have a baseline fitness  $f_W = 1$  and mutant cells have fitness  $f_M = 1 + s$ . We assume  $0 < s \ll 1$ , giving  $M$  a small selective advantage over  $W$ .

The microbial metapopulation can be envisioned as a graph whose nodes  $x \in \{1, \dots, \Omega\}$  are demes (also called sites). Each deme is a well-mixed subpopulation of size  $n = n_W + n_M$  located at a node of the metapopulation graph. Here, we focus on fully-connected graphs (as in the island model [33, 34]), called cliques, and periodic one- and two-dimensional lattices called respectively cycles and grids, see Fig. 1(a). These are regular circulation graphs, generally denoted by  $G = \{\text{clique, cycle, grid}\}$ , of  $\Omega$  demes connected by edges to their  $q_G$  nearest neighbours via cell migration at per capita rate  $m$  (independently from division and death) [33, 34, 41–43, 60], see Fig. 1(a-c). We study the eco-evolutionary dynamics of the metapopulation in the biologically relevant regime of slow migration [41, 42, 61–63], see Appendix B, and consider that initially one deme is occupied entirely by mutants ( $M$  deme), while the other  $\Omega - 1$  demes ( $W$  demes) are all populated by  $W$  cells, see Sec. V. All demes are assumed to have the same carrying capacity  $K$  which encodes environmental variability. In Sec. III, we assume that  $K$  is constant, and in Sec. IV we let the carrying capacity switch endlessly between two values representing mild and harsh conditions [16–24, 32], see below.

In close relation to the Moran process [64–67] (see Appendix B), a reference model in mathematical biology [7], the intra-deme dynamics in a deme  $x$  is thus represented by a multivariate birth-death process defined by birth and death of a cell of type  $\alpha \in \{W, M\}$  in that site according to the reactions [16, 17, 22, 32]

$$n_\alpha \xrightarrow{T_\alpha^+} n_\alpha + 1 \quad \text{and} \quad n_\alpha \xrightarrow{T_\alpha^-} n_\alpha - 1, \quad (1)$$

occurring at the transition rates

$$T_\alpha^+(x) = \frac{f_\alpha}{\bar{f}} n_\alpha \quad \text{and} \quad T_\alpha^-(x) = \frac{n}{K} n_\alpha, \quad (2)$$

where  $\bar{f} \equiv (n_W f_W + n_M f_M)/n$  is the the average fitness in deme  $x$ , and  $K$  here denotes the constant carrying capacity in a static environment and its time-switching version in a dynamical environment, see below. In this formulation, without loss of generality, selection operates on birth events. This can be generalised to include selection on deaths, see e.g. [10, 11].

The inter-deme dynamics stems from the migration of one cell of type  $\alpha \in \{W, M\}$  from the site  $x$  to one of its  $q_G$  neighbouring demes denoted by  $y$  at a per-capita migration rate  $m$ . Here, for the sake of simplicity, we assume that the migration rate is the same in all directions

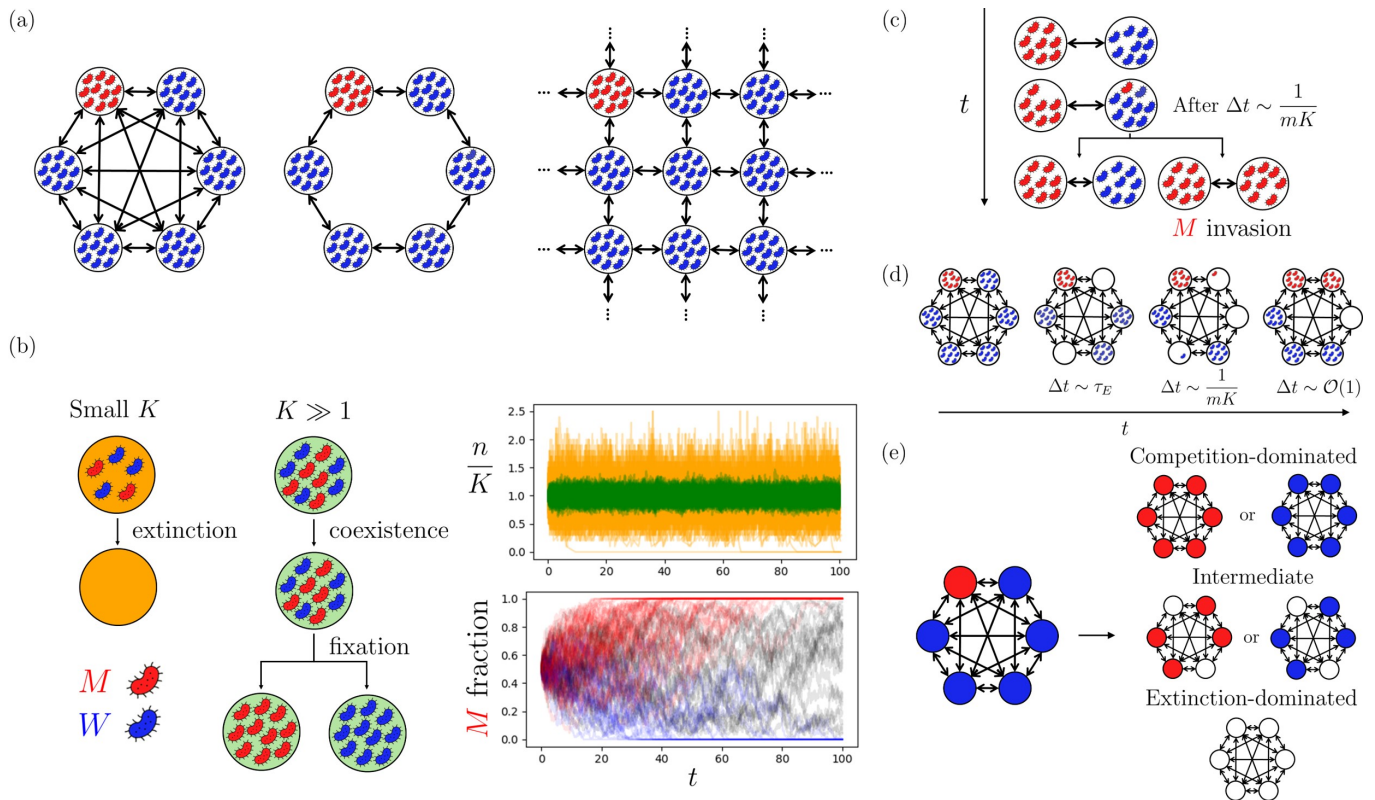


FIG. 1. Metapopulation dynamics in a static environment. (a) *Examples of metapopulation graphs*: a clique, cycle, and grid (from left to right). Neighbouring demes are connected by migration (double arrows). Initially, there is one mutant deme (red/light) and  $\Omega - 1$  wild-type demes (blue / dark), and all demes have the same constant carrying capacity  $K$ . (b) *Dynamics in a single deme*. Left: Wild-type  $W$  cells (blue / dark) compete with mutants of type  $M$  (red / light). When  $K$  is small, the deme is prone to extinction. When  $K$  is large, both types coexist prior to  $W$  or  $M$  fixation. Top, right: Several realisations of the rescaled deme size  $n/K$  vs. time  $t$  for  $K = 5$  (orange/light) and  $K = 100$  (green/dark). Bottom, right: Fraction of  $M$  cells vs.  $t$  in a deme with  $K = 100$ . Deme extinction is not observed. Transient coexistence of  $W$  and  $M$  is followed by the fixation of  $W$  (blue traces) or  $M$  (red traces). Here  $s = 0.01$ . (c) *Invasion of  $W$  deme by an  $M$  cell*: An  $M$  cell migrates to a neighbouring  $W$  deme with migration rate  $m$  after a mean time  $\Delta t = 1/(mK)$ , and then either quickly fixes, producing a new  $M$  deme (right), or does not fix leaving the pair of  $M$  and  $W$  demes unchanged (left). The same picture holds for the invasion of an  $M$  deme by a  $W$  cell, see text. (d) *Intermediate regime* (here for the clique): The dynamics is characterised by deme extinction and  $W/M$  competition (see text). Deme extinction occurs after a mean time  $\tau_E$ , and empty demes are then recolonised by an invader from a neighbouring surviving deme after  $\Delta t \sim 1/(mK)$ . A recolonised deme is rapidly taken over (in  $\Delta t \sim \mathcal{O}(1)$ ). (e) *Coarse-grained description of the metapopulation dynamics*: Each deme is always either fully  $W$  (blue / dark) or  $M$  (red / light) or empty (white). In this description, different scenarios arise, shown for the clique. Competition-dominated regime: all demes are occupied and there is always fixation of  $W$  or  $M$ . Intermediate regime: eventually  $W$  or  $M$  take over all occupied demes, resulting in a dynamic equilibrium of empty demes and  $W$  or  $M$  demes, see text. Extinction-dominated regime: there are frequent deme extinctions and the metapopulation quickly goes extinct.

and for both types (symmetric migration) (see Sec. V for a discussion of these assumptions). The inter-deme dynamics for all cells at deme  $x$  with its neighbouring demes labelled  $y$  is therefore implemented according to the reaction

$$[n_\alpha(x), n_\alpha(y)] \xrightarrow{T_\alpha^{m,G}} [n_\alpha(x) - 1, n_\alpha(y) + 1], \quad (3)$$

occurring at the migration transition rate

$$T_\alpha^{m,G}(x) = \frac{mn_\alpha}{q_G}. \quad (4)$$

Microbial communities generally live in time-varying

conditions, and are often subject to sudden and drastic environmental changes. Here, environmental variability is encoded in the time-variation of the binary carrying capacity [16–24, 32]

$$K(t) = \frac{1}{2} [K_- + K_+ + \xi(t)(K_+ - K_-)]. \quad (5)$$

driven by a random telegraph process  $\xi(t) \in \{-1, 1\}$ . The coloured dichotomous Markov noise (DMN)  $\xi(t)$  switches between  $\pm 1$  according to  $\xi \rightarrow -\xi$  at rate  $\nu$  for the symmetric DMN (see Secs. V and H for the generalisation to asymmetric switching) [68–70]. The carrying capacity, equal across demes, thus switches at a

rate  $\nu$  between a value  $K = K_+$  in a mild environment (e.g. abundance of nutrients, lack of toxin) and  $K = K_- < K_+$  under harsh environmental conditions (e.g. lack of nutrients, abundance of toxin) according to  $K_- \xrightleftharpoons{\nu} K_+$ , and thus represents random cycles of mild and harsh conditions (feast and famine cycles). The randomly time-switching  $K(t)$  drives the size of each deme, and is hence responsible for the coupling of demographic fluctuations with environmental variability, an effect particularly important when there are population bottlenecks [18, 19, 21–24, 32], see below. Here, the DMN is at stationarity and therefore its average vanishes,  $\langle \xi(t) \rangle = 0$ , and its autocovariance coincides with its autocorrelation reading  $\langle \xi(t)\xi(t') \rangle = e^{-2\nu|t-t'|}$  [68–70], where  $\langle \cdot \rangle$  denotes the ensemble average and  $1/(2\nu)$  is the finite correlation time. This implies that the fluctuating carrying capacity is always at stationarity, with a constant average  $\langle K(t) \rangle = \langle K \rangle = (K_+ + K_-)/2$  and an autocorrelation  $\langle K(t)K(t') \rangle = \langle K \rangle e^{-2\nu|t-t'|}$ . In our simulations with symmetric random switching, the carrying capacity is initially drawn from its stationary distribution, with  $K(0) = K_+$  or  $K(0) = K_-$  each with probability  $1/2$ , see Secs. V and H.

The full individual-based model is therefore a continuous-time multivariate Markov process defined by the reaction and transition rates Eqs. (1)–(4) that satisfies the master equation Eq. (A2) discussed in Appendix A 1. The microscopic intra- and inter-deme dynamics encoded in the master equation (A2) has been simulated using the Monte Carlo method described in Appendix I. The eco-evolutionary dynamics of a single deme is outlined in Appendix A 2. It is worth noting that  $n, n_W$ , and  $n_M$  are all fluctuating quantities that depend on the site  $x$  and time  $t$ , and on  $\xi$  in a time-varying environment. However, for notational simplicity, we often drop the explicit dependence on some or all of the variables  $x, t$ , and  $\xi$ . Below, we combine coarse-grained analytical approximations and individual-based stochastic simulations to study how the spatial structure, migration, and demographic fluctuations influence the fixation and extinction properties of the microbial metapopulation.

### III. STATIC ENVIRONMENTS

We first consider a static environment where the carrying capacity  $K$  of each deme is constant. In this setting, the size of each deme rapidly reaches  $K$ , with  $n \approx K$ , see Fig. 1(b), and the expected number of migrants per unit time and deme is  $mK$ . The occurrence of migration events, alongside the competition between  $M$  and  $W$  to take over demes of the other type, increases with  $K$ . Cell migration and competition are however limited when  $K$  is small: regardless of their type, demes of small size are prone to extinction in a mean time  $\tau_E(K)$ , see Fig. 1(b,d). For independent demes of size  $K$ , the deme mean extinction time  $\tau_E(K)$  can be obtained from a lo-

gistic birth-death process, see Appendix C, yielding

$$\tau_E(K) \approx \frac{e^K}{K}, \quad (6)$$

when  $K \gg 1$ , see Fig. 2(e). In our analysis, we distinguish between different dynamical scenarios through

$$\psi(m, K) \equiv mK\tau_E, \quad (7)$$

giving the average number of migration events during the typical deme extinction time. With Eq. (6), we have  $\psi(m, K) \approx m e^K$  when  $K \gg 1$ . In the regime where  $\psi \gg 1$ , many migration events occur before any deme extinction, and the dynamics is thus dominated by  $M/W$  competition. When  $\psi(m, K) < 1$ , migration is ineffective and there is fast extinction of all demes. An intermediate regime where some demes are empty and others occupied by  $W$  or  $M$  arises when  $\psi(m, K) \gtrsim 1$ . To rationalise this picture in the coarse-grained description of Ref. [59], it is useful to track the number of occupied demes  $j = 0, 1, \dots, \Omega$  (by either  $W$  or  $M$  cells). For cliques, as shown in Appendix D, we find that the long-time fraction of occupied demes is

$$\frac{j}{\Omega} \rightarrow \frac{\Omega_{\text{occ}}(m, K)}{\Omega} \approx \begin{cases} 1 & \text{if } \psi \gg 1, \\ \frac{\psi-1}{\psi} & \text{if } \psi \gtrsim 1, \\ 0 & \text{if } \psi < 1. \end{cases} \quad (8)$$

The expression of  $\Omega_{\text{occ}}$  ignores spatial correlations and hence is not accurate for cycles and grids if  $\psi(m, K)$  is not much larger than 1. However,  $\psi(m, K)$  allows us to efficiently distinguish between the regimes dominated by  $M/W$  competition, deme extinction, and the crossover intermediate regime, see Fig. 9 and Appendix D.

Henceforth, we refer to “invasion” when a cell of type  $M/W$  migrates to and fixates in a  $W/M$  deme, and to “recolonisation” when a cell of either type migrates into an empty deme and takes it over, see Fig. 1(c,d). Accordingly, the competition-dominated and intermediate regimes are respectively characterised by invasions and recolonisations, see Fig. 1(c,d).

#### 1. Competition-dominated dynamics

When  $\psi \gg 1$  and  $m \ll 1$ , the carrying capacity is large enough for many migrations to occur on the timescale  $\tau_E$  of deme extinction. Since every deme expects many incoming cells in time  $\tau_E$ , deme extinction is unlikely and can be neglected. In this regime, the dynamics is dominated by local  $M/W$  competition:  $W$  and  $M$  cells compete in each deme to fixate the local subpopulation, see Fig. 1(b).

As in Refs. [41, 42, 51], we can adopt a coarse-grained description treating each deme as a single entity of type  $W$  or  $M$ . In doing so, we assume that migration is slow so that the mean time for an  $M$  or  $W$  invader to fixate in a deme is negligible compared to  $1/(mK)$ , the expected

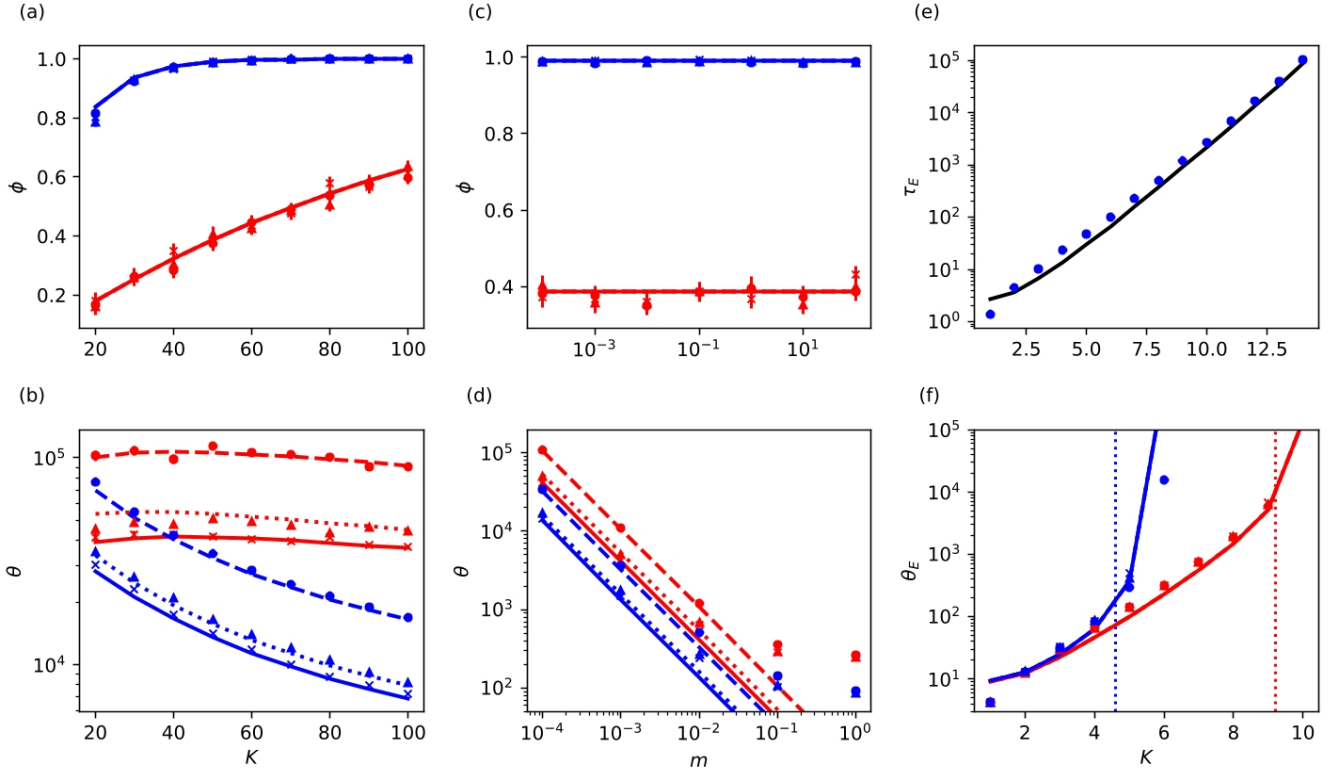


FIG. 2. (a-d): *Competition-dominated dynamics*,  $\psi \gg 1$ . (a)  $M$  fixation probability  $\phi$  vs. constant carrying capacity  $K$ ; (b) unconditional mean fixation time  $\theta$  vs.  $K$ ; (c)  $\phi$  vs. per capita migration rate  $m$ ; (d)  $\theta$  vs.  $m$ . Markers are simulation results and lines are predictions of Eq. (12) for  $s = 0.1$  (blue) and  $s = 0.01$  (red) on a clique (solid lines / crosses), cycle (dashed lines / circles), and grid (dotted lines / triangles). In (a,b),  $m = 10^{-4}$ ,  $\Omega = 16$ , and in (c,d),  $K = 50$ ,  $\Omega = 16$ . In (a,c), markers for the same  $s$  are almost indistinguishable indicating independence of the spatial structure. (e,f): *Extinction-dominated dynamics*,  $\psi < 1$ . (e) Mean extinction time of a single deme  $\tau_E$  vs.  $K$  ( $m = 0$ ). Blue circles are simulation data, black line line shows the predictions of Eq. (6). (f) Metapopulation mean extinction time  $\theta_E$  vs.  $K$  for  $\Omega = 16$  and  $m = 10^{-2}$  (blue) and  $10^{-4}$  (red). Markers are simulation results and thick lines are predictions of Eq. (C4) for cliques (solid lines / crosses), cycles (dashed lines / circles), and grids (dotted lines / triangles). Thin dashed vertical lines are guides to the eye showing  $\psi = 1$  for  $m = 10^{-2}$  (blue) and  $10^{-4}$  (red). Selection plays no role in this regime, so panels (e,f) have been obtained with  $s = 0$ . In all panels, there is initially one  $M$  deme and  $\Omega - 1$  demes occupied by  $W$ . Error bars are plotted in each case but are typically too small to see.

time between migrations, see Appendix C. In this regime, each sequential migration is an invasion attempt, with a cell from an  $M/W$  site trying to invade a neighbouring  $W/M$  deme, see Fig. 1(c). Here, an  $M/W$  invasion is the fixation of a single  $M/W$  mutant in a deme consisting of  $K - 1$  cells of type  $W/M$ .

In the realm of the coarse-grained description, the state of the metapopulation in this regime is denoted by  $i$ , where  $i = 0, 1, \dots, \Omega$  is the number of demes of type  $M$  leaving  $\Omega - i$  demes of type  $W$ . The probability  $\rho_{M/W}$  of invasion by an  $M/W$  migrant is here given by the probability that a single  $M/W$  cell takes over a population of constant size  $K$  in a Moran process [7, 64–67] and, as shown in Appendix B, reads

$$\begin{aligned} \rho_M(K) &= \frac{1}{1+s} \left[ \frac{s}{1 - (1+s)^{-K}} \right], \\ \rho_W(K) &= \frac{1}{(1+s)^K} \left[ \frac{s}{1 - (1+s)^{-K}} \right]. \end{aligned} \quad (9)$$

In each time unit, a deme receives from and sends to its neighbours an average of  $mK$  cells. Importantly, only edges connecting  $M$  and  $W$  demes can lead to invasions, see Fig. 1(c). These are “active edges” and their number in state  $i$  on graph  $G$  is denoted by  $E_G(i)$ , where here we consider  $G = \{\text{clique}, \text{cycle}, \text{grid}\}$ . Moreover, migration from a deme can occur to any of the  $q_G$  neighbours of the deme, where  $q_{\text{clique}} = \Omega - 1$ ,  $q_{\text{cycle}} = 2$ ,  $q_{\text{grid}} = 4$ , and  $q_{d\text{-dim}} = 2d$  for a  $d$ -dimensional regular lattice, see Eq. (A1). The number of active edges generally varies with the metapopulation state and the spatial structure, and is difficult to determine. However, a clique being the fully-connected graph, the  $i$  demes of type  $M$  are connected to the  $\Omega - i$  demes of type  $W$ , yielding  $E_{\text{clique}}(i) = i(\Omega - i)$ . For a cycle, if the initial state is  $i = 1$ , the initial  $M$  deme is exactly connected to two  $W$  demes. This property is conserved by the coarse-grained dynamics, with an unbreakable cluster of  $M$  demes al-

ways connected to a cluster of  $W$  demes by two active edges until  $W$  or  $M$  fixes the metapopulation, yielding  $E_{\text{cycle}}(i) = 2$  for  $i \neq 0, \Omega$ , see Fig. 1(a,c) and below. The number of active edges in a grid is difficult to find due to complex spatial correlations, but in Appendix E, we show that its average starting from the metapopulation state  $(i, \Omega - i) = (1, \Omega - 1)$ , can be approximated by  $2\sqrt{\pi i}$ . We will therefore approximate  $E_{\text{grid}}(i) \approx 2\sqrt{\pi i}$  for  $i \neq 0, \Omega$ . When  $i = 0, \Omega$ , one strain fixates the entire metapopulation, where all demes are  $M$  if  $i = \Omega$  and all demes are  $W$  when  $i = 0$ , and hence  $E_G(0) = E_G(\Omega) = 0$ .

In the coarse-grained description of the competition-dominated dynamics, starting from a single  $M$  deme ( $i = 1$ ), there are  $mK E_G(i)/q_G$  expected migration attempts to grow an unbreakable cluster of connected  $M$  demes by invading neighbouring  $W$  demes. Since the probability of an  $M$  invasion is  $\rho_M$ , given by Eq. (9), the  $M$ -cluster grows at a rate  $mK E_G(i)\rho_M/q_G$ . Similarly a  $W$  invader attempts to grow an unbreakable  $W$ -cluster by invading  $M$  demes, hence reducing the size of the  $M$  cluster, at a rate  $mK E_G(i)\rho_W/q_G$ . In this representation,  $M$  and  $W$  invasions therefore act at the interface of an unbreakable cluster of  $M$  demes by increasing or reducing its size  $i$  at respective rates [41, 42, 60],

$$\begin{aligned} T_i^+(m, G, K) &= mK \frac{E_G(i)}{q_G} \rho_M, \\ T_i^-(m, G, K) &= mK \frac{E_G(i)}{q_G} \rho_W. \end{aligned} \quad (10)$$

The coarse-grained competition-dominated dynamics is thus a birth-death process for the  $M$ -cluster size  $i$ , with absorbing boundaries at  $i = \Omega$  ( $M$  fixation) and  $i = 0$  ( $W$  fixation), see Appendix G. In this representation, the  $M$  fixation probability in a metapopulation of size  $\Omega$ , spatially structured as a graph  $G$ , consisting initially of  $i$  mutant demes is denoted  $\phi_i^G$ , and the unconditional (i.e. regardless of whether  $M$  or  $W$  takes over [7, 66, 67]) mean fixation time (uMFT) denoted  $\theta_i^G$ . These quantities satisfy the first-step equations [7, 66, 67, 71]

$$\begin{aligned} (T_i^+ + T_i^-)\phi_i^G &= T_i^+\phi_{i+1}^G + T_i^-\phi_{i-1}^G, \\ (T_i^+ + T_i^-)\theta_i^G &= 1 + T_i^+\theta_{i+1}^G + T_i^-\theta_{i-1}^G, \end{aligned} \quad (11)$$

for  $i = 1, \dots, \Omega - 1$ , with boundary conditions  $\phi_0^G = 1 - \phi_\Omega^G = 0$  and  $\theta_0^G = \theta_\Omega^G = 0$ . Eqs. (11) can be solved exactly [66, 67] (see also Appendix B). Here, we are chiefly interested in the fixation of a single initial  $M$  deme,  $i = 1$ , and simply write  $\phi^G \equiv \phi_1^G$  and  $\theta^G \equiv \theta_1^G$ , finding

$$\begin{aligned} \phi^G(K) &= \phi(K) = \frac{1 - \gamma}{1 - \gamma^\Omega}, \\ \theta^G(m, G, K) &= \frac{1 - \gamma}{1 - \gamma^\Omega} \sum_{k=1}^{\Omega-1} \sum_{n=1}^k \frac{\gamma^{k-n}}{T_n^+(m, G, K)}, \end{aligned} \quad (12)$$

where  $\gamma \equiv T_i^-/T_i^+ = \rho_W/\rho_M \approx \exp(-Ks)$  is a quantity independent of  $m$  and  $G$ . As noted in Refs. [41, 42, 50]

the fixation probability  $\phi^G = \phi$  is therefore independent of the migration rate and spatial structure. This remarkable result stems from the graphs considered here being *circulations*: There is the same incoming and outgoing migration flow at each deme. In *static environments*, a generalised circulation theorem ensures that the fixation probability is independent of  $m$  and  $G$  for circulation graphs [41, 42, 47], a feature displayed in the stochastic simulations of Fig. 2(a,c) for the full microscopic model. In excellent agreement with simulation data of Fig. 2(a,c), we find that the  $M$  fixation probability increases almost exponentially and approaches 1 when  $Ks \gg 1$ ,  $\phi^G \approx 1$ . This stems from the invasion of  $W$  demes being increasingly likely (and the invasion of  $M$  demes exponentially less likely) when the average number of migrations ( $mK$ ) increases along with  $K$ . When  $Ks \ll 1$ , the competition is effectively neutral, and in this case  $\phi^G \approx 1/\Omega$ . In good agreement with simulation results of Fig. 2(b,d), Eq. (12), predicts that the uMFT decreases with the migration rate  $\theta^G \sim 1/m$  and, for given parameters, the uMFT is shortest on cliques, while it is larger on cycles than on grids. Intuitively, for higher  $m$  and more connected graphs, migrants spread faster leading to quicker invasion and fixation.

## 2. Extinction-dominated dynamics

In the extinction-dominated regime  $\psi < 1$  with  $m \ll 1$ , we do not expect any deme invasions in a time  $\tau_E$ . Therefore, the timescale of extinction dynamics is much shorter than that of  $M/W$  competition, and site extinction dominates over deme invasion, see Fig. 1e. The dynamics in this extinction-dominated regime is governed by the random extinction of demes, regardless of their type. Following Ref. [59], in the realm of the coarse-grained description outlined in Appendix C, demes are regarded as being either occupied (by either  $W$  or  $M$  cells) or empty. Deme extinction occurs randomly while empty demes may be recolonised by migrations from occupied neighbouring demes. The coarse-grained dynamics is thus independent of the spatial structure, and can be represented by a birth-death process for the number of occupied demes, assuming that the site extinction and recolonisation occur instantaneously [59], see Appendix C. In this coarse-grained representation, when all demes are initially occupied ( $n = K$ ), the metapopulation mean extinction time (mMET) is given by Eq. (C4) in Appendix C. When  $\Omega \gg 1$  and  $\psi < 1$ , the leading contribution to the mMET arises from the term  $i = n$  in the innermost sum, yielding

$$\theta_E(K, \Omega) \approx \tau_E(\ln(\Omega) + \gamma_{\text{EM}}), \quad (13)$$

where  $\gamma_{\text{EM}} \approx 0.577\dots$  is the Euler-Mascheroni constant. Eq. (13) gives a good approximation of the mMET. As  $\psi$  increases with  $K$ , at the upper-limit of the extinction-dominated limit (where  $\psi$  approaches 1), the mMET grows almost exponentially with  $K$  and logarithmically with  $\Omega$ ,  $\theta_E \approx e^K \ln(\Omega)/K$ . Eq. (C4) thus predicts a

rapid growth of the mMET when  $\psi \gtrsim 1$ , as shown in Fig. 2(f,g) where simulation results are found to be in good agreement with Eq. (C4).

### 3. Intermediate dynamics

In the intermediate regime  $\psi \gtrsim 1$  and  $m \ll 1$ , there is a crossover between the extinction and competition-dominated dynamics. At fixed migration rate  $m$ , this crossover regime occurs in the range  $\ln(1/m) \lesssim K \lesssim \ln(\Omega K/m)$ . Furthermore, the metapopulation is partially occupied for  $\ln(1/m) \lesssim K \lesssim \ln(\Omega/m)$  corresponding to  $1 < \psi < \Omega - 1$ . These bounds are illustrated by the vertical lines in Fig. 11.

When  $\psi \gtrsim 1$ , migration and deme extinction occur on the timescale  $\tau_E$ . In the long run, deme recolonisations and extinctions balance each other, yielding a dynamical equilibrium consisting of  $\Omega_{\text{occ}} = \Omega(1 - 1/\psi)$  occupied demes and  $\Omega - \Omega_{\text{occ}}$  empty demes, see Fig. 9. In this regime, the three-state coarse-grained description of the dynamical equilibrium consists of a random mixture of empty demes, and occupied  $W$  and  $M$  demes, see Fig. 1(d). After a mean time  $\theta_{\text{int}}^G$  the metapopulation reaches the dynamical equilibrium consisting of a fraction  $1 - \Omega_{\text{occ}}/\Omega = 1/\psi$  empty demes, and the remaining demes are all of either type  $M$  or  $W$  with probability  $\phi_{\text{int}}^G$  and  $1 - \phi_{\text{int}}^G$ , respectively. The dynamical equilibrium is thus defined by the quantities  $\psi$ , given by Eq. (7), and  $\phi_{\text{int}}^G$  which is the probability that mutants  $M$  take over the  $\Omega_{\text{occ}} = \Omega(1 - 1/\psi)$  occupied demes in a mean time  $\theta_{\text{int}}^G$ . These quantities are derived and discussed in Appendix F for a metapopulation on an arbitrary regular lattice consisting initially of a single  $M$  deme, see (F3) and Fig. 11

## IV. TIME-FLUCTUATING ENVIRONMENTS

Microbial populations generally evolve in time-varying environments, and are often subject to conditions changing suddenly and drastically, e.g. experiencing cycles of harsh and mild environmental states [20, 28, 30, 72–83], see Fig. 3. These variations cause fluctuations often associated with population *bottlenecks*, arising when the deme size is drastically reduced, e.g. due to nutrient scarcity or exposure to toxins [27–29, 31, 77]. Here, environmental variability is encoded in the time-fluctuating carrying capacity  $K(t)$  (5) driven by the DMN  $\xi(t) \in \{-1, 1\}$  [16–24, 32, 68–70], see Sec. II. Hence, when  $\nu \lesssim 1$ , the deme size  $n$  tracks  $K(t)$  and experiences a bottleneck whenever the carrying capacity switches from  $K_+$  to  $K_-$ , see Appendix A 2 and Fig. 3(a,right) [16–18].

In order to study the joint effect of migration and fluctuations on the metapopulation dynamics, we assume  $K_+ \gg 1$  such that demographic fluctuations are weak in the mild environment. In what follows, we distinguish between weak bottlenecks, where  $\psi(m, K_-) \gg 1$

and deme extinction is negligible, and strong bottlenecks, where  $\psi(m, K_-) < 1$  and deme extinctions dominate.

### 1. Weak bottlenecks: $\psi(m, K_-) \gg 1$

When  $K_+ > K_-$  with  $\psi(m, K_-) \gg 1$ , each deme experiences a weak bottleneck at an average frequency  $\nu/2$  when  $\nu \lesssim 1$ , see Fig. 3(a,top). The condition  $\psi(m, K_-) \approx me^{K_-} \gg 1$  ensures that deme extinction can be neglected, with metapopulation dynamics dominated by  $M/W$  competition. The metapopulation fate can thus be captured by a two-state coarse-grained description similar to that of Sec. III 1. Since the deme size in the environment  $\xi$ , and hence the number of migrating cells, varies with  $K(t)$ , it is useful to introduce the long-term average deme size in environmental state  $\xi = \pm 1$  under switching rate  $\nu$  denoted by  $\mathcal{N}_\xi(\nu) \equiv \mathcal{N}_\pm(\nu)$ , see below.

We first discuss the metapopulation fate in the limit of slow and fast environmental switching, and then return to the above case of intermediate switching.

When the environment varies very slowly,  $\nu \ll 1$ , the carrying capacity remains at its initial value, i.e.  $K(t) = K_+$  or  $K(t) = K_-$  each with a probability 1/2, until invasions lead to the fixation of  $W$  or  $M$ . In the slow switching regime, the  $M$  fixation probability and uMFT on a metapopulation spatially arranged as a regular graph  $G$  are respectively denoted by  $\Phi_0^G$  and  $\Theta_0^G$ . The quantities are obtained by averaging their static counterparts (12) over the stationary distribution of  $K$ , yielding for symmetric switching

$$\begin{aligned} \Phi_0^G(m, K_\pm) &= \Phi_0(K_\pm) = \frac{1}{2} [\phi(K_+) + \phi(K_-)], \\ \Theta_0^G(m, K_\pm) &= \frac{1}{2} [\theta^G(m, K_+) + \theta^G(m, K_-)]. \end{aligned} \quad (14)$$

When the environment varies very quickly,  $\nu \gg 1$ , the DMN self averages before invasion-mediated fixation occurs, and the carrying capacity of each deme rapidly reaches the effective value

$$\mathcal{K} \equiv \frac{2K_+K_-}{K_+ + K_-}, \quad (15)$$

the harmonic mean of  $K_+$  and  $K_-$ , with  $\mathcal{N}_\pm(\infty) \rightarrow \mathcal{K}$  [16–18, 22], see Appendix A 2. In this fast switching regime, the  $M$  fixation probability and uMFT on a metapopulation spatially arranged as a regular graph  $G$ , respectively denoted by  $\Phi_\infty^G$  and  $\Theta_\infty^G$ , are obtained by replacing  $K$  with  $\mathcal{K}$  in Eq. (12), yielding

$$\begin{aligned} \Phi_\infty^G(m, \mathcal{K}) &= \Phi_\infty(\mathcal{K}) = \phi(\mathcal{K}), \\ \Theta_\infty^G(m, K_\pm) &= \theta^G(m, \mathcal{K}). \end{aligned} \quad (16)$$

From these expressions and Eq. (12), we notice the fixation probability in the regime of slow and fast switching is independent of the migration rate and spatial structure:



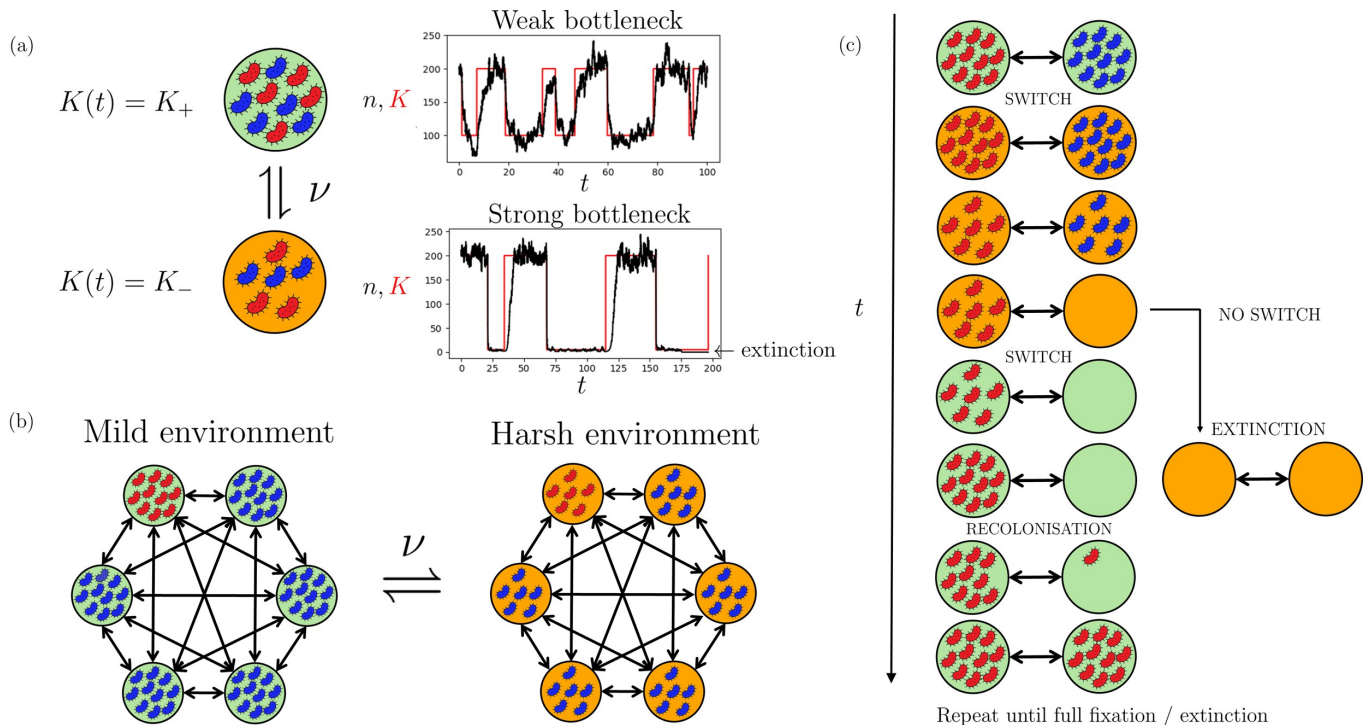


FIG. 3. (a) Left: single deme in time-switching environment. The carrying capacity  $K(t)$  encodes environmental variability by switching between  $K = K_+$  (mild environment, green / light) and  $K(t) = K_- < K_+$  (harsh environment, orange / dark) at symmetric rate  $\nu$  (see also Appendix H). Communities are larger in the mild environment. When  $K(t)$  switches at an intermediate rate, each deme experiences bottlenecks at an average frequency  $1/(2\nu)$ . Right:  $n$  and  $K$  vs. time in the intermediate switching regime where the size  $n$  of a deme undergoes bottlenecks. Parameters are:  $K_+ = 200$ ,  $\nu = 0.05$  and  $K_- = 100$  (top) and  $K_- = 5$  (bottom). The bottlenecks are weak when  $\psi(m, K_-) \gg 1$  (top, right) where deme extinction is unlikely. When  $\psi(m, K_-) < 1$ , there are strong bottlenecks and each deme can go extinct in the harsh environment (bottom, right). (b) Cliques metapopulation with  $\Omega = 6$  connected demes (double arrows). All demes have the same time-switching carrying capacity  $K(t)$  encoding environmental variability across the metapopulation, with each deme in the same environmental state. (c) Example evolution across two nearest-neighbour demes in a switching environment subject to strong bottlenecks in the intermediate switching regime, see text. Starting in the mild environment where  $K = K_+$ , the carrying capacity switches to  $K_-$  (harsh environment) after  $t \sim 1/\nu$ . Following the  $K_+ \rightarrow K_-$  switch, each deme size decreases and each subpopulation is subject to strong demographic fluctuations and hence prone to extinction. In the absence of recolonisation of empty demes, effective only in the mild state, all demes go extinct. If there is a switch back to the mild environment  $K_- \rightarrow K_+$  prior to total extinction, empty demes can be rescued by migration and recolonised by incoming  $W$  or  $M$  cells from neighbouring demes. In the sketch, an empty deme is recolonised by a mutant in the mild environment and becomes an  $M$  deme. The cycle continues until the entire metapopulation consists of only  $W$  or  $M$  demes, or metapopulation extinction.

$\Phi_0^G = \Phi^0$  and  $\Phi_\infty^G = \Phi_\infty$ . However, the metapopulation uMFT depends explicitly on the migration rate  $m$  and  $G$ , with  $\Theta_0^G \sim 1/m$  and  $\Theta_\infty^G \sim 1/m$ .

Under intermediate switching rate, when  $\nu \lesssim 1$ , the coupling of demographic and environmental fluctuations plays a key role, while cell migration depends on the deme size that in turn varies with the environmental state. Here, the metapopulation dynamics cannot be directly related to its static counterpart. The average deme size  $\mathcal{N}_\xi(\nu)$  depends non-trivially on  $\nu$  and  $\xi$ , and generally needs to be computed by sampling long-time simulations. However, analytical progress can be made by approximating the population size distribution of an isolated deme in the environmental state  $\xi$  by the joint probability density  $p_\xi(\nu, n)$  of the piecewise deterministic Markov process (PDMP) obtained by ignoring demographic fluc-

tuations [16, 17, 84, 85], see Appendix A 2

$$p_\xi(\nu, n) = \begin{cases} \frac{\mathcal{Z}_+}{n^2} \left(\frac{K_+ - n}{n}\right)^{\nu-1} \left(\frac{n - K_-}{n}\right)^\nu & \text{if } \xi = 1, \\ \frac{\mathcal{Z}_-}{n^2} \left(\frac{K_+ - n}{n}\right)^\nu \left(\frac{n - K_-}{n}\right)^{\nu-1} & \text{if } \xi = -1. \end{cases} \quad (17)$$

The density  $p_\xi(\nu, n)$  has support  $[K_-, K_+]$ , and the normalisation constants  $\mathcal{Z}_\pm$  ensure  $\int_{K_-}^{K_+} p_\xi(\nu, n) dn = 1$ . The  $M/W$  competition characterising the intermediate switching regime dynamics can be described by the coarse-grained representation of Sec. III 1 generalised to a time-fluctuating environment following Refs. [16, 17, 22]. Here, we analyse the influence of  $\nu$  and  $m$  on the  $M$  fixation probability,  $\Phi_i^G(\nu, m)$ , and uMFT,  $\Theta_i^G(\nu, m)$ , in a metapopulation consisting of  $i$  mutants demes and  $\Omega - i$   $W$ -demes spatially arranged as a regular graph  $G$ .



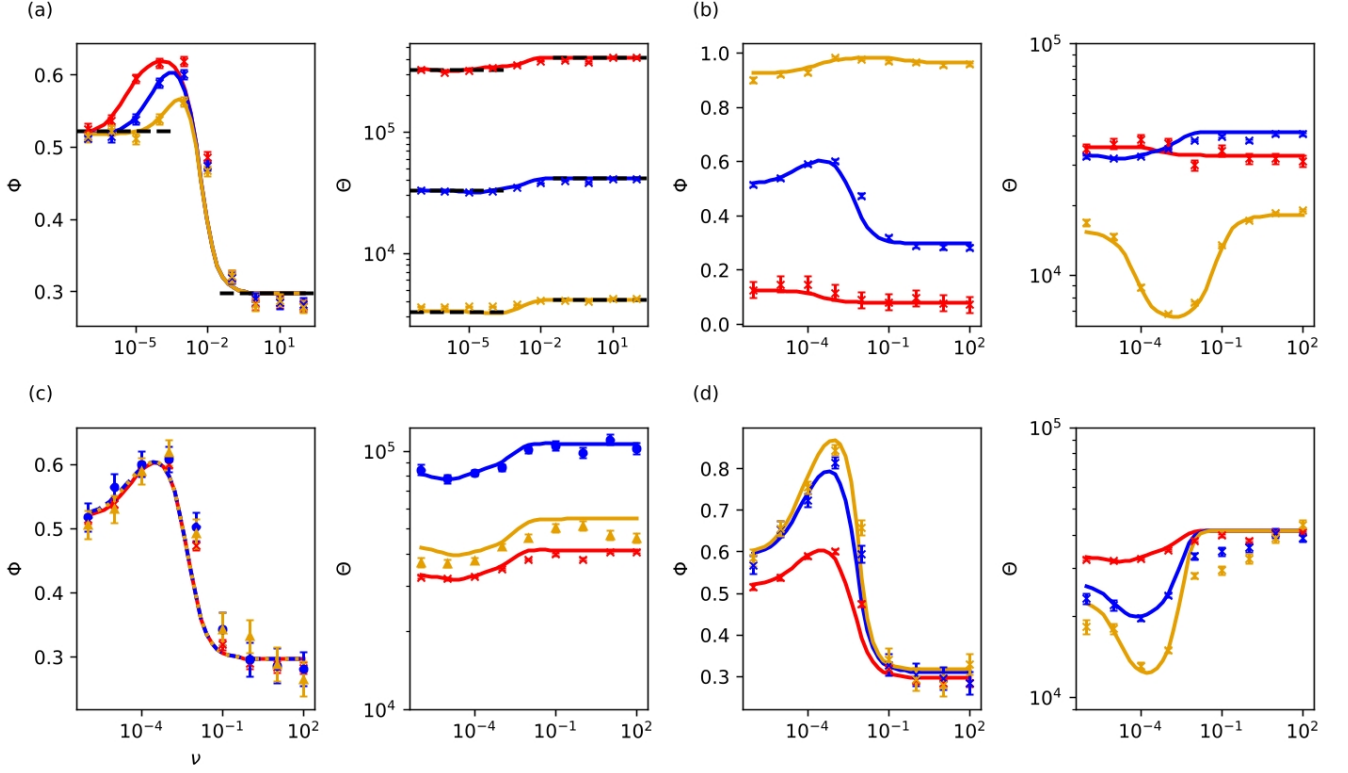


FIG. 4. Fixation probability  $\Phi^G$  and mean fixation time  $\Theta^G$  against switching rate  $\nu$  for various parameters. Each panel shows  $\Phi^G$  vs.  $\nu$  (left) and  $\Theta^G$  vs.  $\nu$  (right). Markers show simulation results and lines are predictions of Eq. (24). (a,b)  $\Phi^{\text{clique}}(\nu)$  and  $\Theta^{\text{clique}}(\nu)$  for a clique metapopulation and different values of  $m$  in (a) and  $s$  in (b). (a)  $m = 10^{-5}$  (red),  $m = 10^{-4}$  (blue),  $m = 10^{-3}$  (yellow), and  $s = 0.01$ . (b)  $s = 10^{-3}$  (red),  $s = 10^{-2}$  (blue),  $s = 10^{-1}$  (yellow), and  $m = 10^{-4}$ . Dashed black lines are guides to the eye showing  $\Phi_{0,\infty}$  in (a,left) and  $\Theta_{0,\infty}$  in (a,right), see text. Other parameters are  $\Omega = 16$ ,  $K_+ = 200$ , and  $K_- = 20$ . (c)  $\Phi^G(\nu)$  and  $\Theta^G(\nu)$  for clique (red, crosses), cycle (blue, circles), and grid (yellow, triangles). Other parameters are  $\Omega = 16$ ,  $K_+ = 200$ ,  $K_- = 20$ ,  $s = 0.01$ ,  $m = 10^{-4}$ . (d)  $\Phi^{\text{clique}}(\nu)$  and  $\Theta^{\text{clique}}(\nu)$  for a clique metapopulation with  $K_+ = 200$  (red),  $K_+ = 500$  (blue), and  $K_+ = 1000$  (yellow). Deviations occur for  $\Theta$  with  $K_+ = 1000$  since the slow-migration condition is not satisfied in the mild environment. Other parameters are  $\Omega = 16$ ,  $K_- = 20$ , and  $s = 0.01$ ,  $m = 10^{-4}$ . In all examples, there is initially a single  $M$  deme and  $\Omega - 1$  others of type  $W$ , see text.

To this end, we consider a birth-death process for the number  $i = 0, \dots, \Omega$  of  $M$  demes forming an  $M$ -cluster. As in Sec. III 1, we assume that there is initially a single  $M$  deme ( $i = 1$ ). The effective rates for increase or decrease in size of the  $M$ -cluster,  $\mathcal{T}_i^\pm$ , depend on the expected number of migrating cells, which in turn depends on the deme size that is now a time-fluctuating quantity driven by Eq. (5). In a time-varying environment, the expected number of migrants from a deme,  $mn$ , is approximated by  $m\mathcal{N}_\xi(\nu)$ , where the long-time mean deme size in the environmental state  $\xi$  is obtained from the PDMP density according to

$$\mathcal{N}_\xi(\nu) = \int_{K_-}^{K_+} np_\xi(\nu/s, n) dn, \quad (18)$$

where, as in Refs. [16–19, 23], the switching rate has been rescaled,  $\nu \rightarrow \nu/s$ , by the timescale of the deme fixation dynamics, see Appendix B, where there are an average of  $\mathcal{O}(\nu/s)$  switches on the deme fixation timescale [17, 18].

The (marginal) average deme size regardless of  $\xi$  is given by  $\mathcal{N}(\nu) = \frac{1}{2} \sum_\xi \mathcal{N}_\xi(\nu)$  and known to be a decreasing function of  $\nu$  [16, 17]. As in static environments, see Eq. (10), the transition rates  $\mathcal{T}_i^\pm$  depend on the spatial structure, via  $E_G(i)/q_G$ , and on the probability  $\rho_{M/W,\xi}(\nu)$  that an  $M/W$  migrant invades a  $W/M$  deme in the environment  $\xi$ . Putting everything together, this yields the effective transition rates

$$\begin{aligned} \mathcal{T}_{i,\xi}^+(\nu, m, G) &= m\mathcal{N}_\xi(\nu) \frac{E_G(i)}{q_G} \rho_{M,\xi}(\nu), \\ \mathcal{T}_{i,\xi}^-(\nu, m, G) &= m\mathcal{N}_\xi(\nu) \frac{E_G(i)}{q_G} \rho_{W,\xi}(\nu), \end{aligned} \quad (19)$$

where, by analogy with Eq. (9), we have introduced

$$\begin{aligned} \rho_{M,\xi}(\nu) &\equiv \frac{s}{1+s} \frac{1}{1 - (1+s)^{-\mathcal{N}_\xi(\nu)}}, \\ \rho_{W,\xi}(\nu) &\equiv \frac{s}{(1+s)^{\mathcal{N}_\xi(\nu)}} \frac{1}{1 - (1+s)^{-\mathcal{N}_\xi(\nu)}}. \end{aligned} \quad (20)$$

With Eq. (19), by dropping all explicit dependence except on  $i$  and  $\xi$ , we obtain the  $M$  fixation probability in the environmental state  $\xi$ , denoted by  $\Phi_{i,\xi}^G(\nu, m, K_{\pm})$ , as the solution of the following  $\nu$ -dependent first-step analysis equation:

$$\left[ \mathcal{T}_{i,\xi}^+ + \mathcal{T}_{i,\xi}^- + \nu \right] \Phi_{i,\xi}^G = \mathcal{T}_{i,\xi}^+ \Phi_{i+1,\xi}^G + \mathcal{T}_{i,\xi}^- \Phi_{i-1,\xi}^G + \nu \Phi_{i,-\xi}^G, \quad (21)$$

subject to the boundary conditions  $\Phi_{0,\xi}^G = 0$  and  $\Phi_{\Omega,\xi}^G = 1$ . The metapopulation uMFT in the environmental state  $\xi$ , denoted by  $\Theta_{i,\xi}^G$ , satisfies a similar equation:

$$\left[ \mathcal{T}_{i,\xi}^+ + \mathcal{T}_{i,\xi}^- + \nu \right] \Theta_{i,\xi}^G = 1 + \mathcal{T}_{i,\xi}^+ \Theta_{i+1,\xi}^G + \mathcal{T}_{i,\xi}^- \Theta_{i-1,\xi}^G + \nu \Theta_{i,-\xi}^G, \quad (22)$$

with boundary conditions  $\Theta_{0,\xi}^G = \Theta_{\Omega,\xi}^G = 0$ . Eqs. (21) and (22) generalise Eqs. (11) to a time-switching environment, with the last terms on the RHS accounting for environmental switching, and coupling  $\Phi_{i,\xi}^G$  to  $\Phi_{i,-\xi}^G$  and  $\Theta_{i,\xi}^G$  to  $\Theta_{i,-\xi}^G$ . Eqs. (21) and (22) can be solved numerically using standard methods. The  $M$  fixation probability  $\Phi_i^G(\nu)$  and uMFT  $\Theta_i^G(\nu)$  regardless of  $\xi$  are obtained by averaging over the stationary distribution of  $\xi$ , yielding

$$\begin{aligned} \Phi_i^G(\nu, m) &= \frac{1}{2} \sum_{\xi} \Phi_{i,\xi}^G(\xi, \nu, m), \\ \Theta_i^G(\nu, m) &= \frac{1}{2} \sum_{\xi} \Theta_{i,\xi}^G(\xi, \nu, m), \end{aligned} \quad (23)$$

where we have reinstated the explicit dependence on  $\nu$  and  $m$ . As we specifically consider the initial condition of a single  $M$  deme, we set  $i = 1$  in Eq. (23) and simplify the notation by writing

$$\Phi^G(\nu, m) = \Phi_1^G(\nu, m) \text{ and } \Theta^G(\nu, m) = \Theta_1^G(\nu, m), \quad (24)$$

Eq. (24) are the expressions of the  $M$  fixation probability and metapopulation uMFT in the realm of the combined coarse-grained and PDMP description. This approach is valid under slow migration rate ( $m \ll 1$ ) and weak selection strength ( $s \ll 1$ ) for the assumption  $n \approx \mathcal{N}_{\xi}(\nu)$  to hold at each invasion, see Appendix A 2. In Fig. 4, the comparison of the predictions of Eq. (24) with the simulation results of the full model on the regular graphs  $G = \{\text{clique, cycle, grid}\}$  shows that (24) captures well the dependence of  $\Phi^G$  and  $\Theta^G$  on  $\nu$ ,  $m$ ,  $s$  and  $K_+$ . In particular, Eq. (24) reproduces on all  $G$  the non-monotonic  $\nu$ -dependence of  $\Phi^G$  and  $\Theta^G$  (when it exhibits this feature), as well as their behaviour when  $\nu \rightarrow 0, \infty$  given by Eqs. (14) and (16).

A striking feature of  $\Phi^G$  and  $\Theta^G$  is their dependence on spatial migration. In Fig. 4(a,left), we indeed find that simulation data for  $\Phi^{\text{clique}}(\nu, m)$  vary noticeably with  $m$  in the range  $\nu \in [10^{-4}, 10^{-1}]$ . These deviations, of up to 20%, exceed the error bars and are reasonably well captured by Eq. (24). In Fig. 4(c,left), we notice that both simulation results and predictions of Eq. (24)

for  $\Phi^G(\nu, m)$  differ slightly for each graph  $G$ , whereas Fig. 4(c,right) shows that  $\Theta^G$  clearly depends on the spatial structure. The explicit dependence of the fixation probability on migration and spatial structure is in stark contrast with the result Eq. (12) obtained in static environments, and is therefore a signature of the eco-evolutionary dynamics in time-fluctuating environments. As shown in Appendix G, the correspondence demonstrated in Ref. [41] between  $\Phi^G$  and the fixation probability of a random walk for the number  $i = 0, 1, \dots, \Omega$  of mutant demes with hopping probabilities independent of  $m$  and  $G$ , and absorbing states  $0, \Omega$ , breaks down in time-varying environments. This leads to the dependence of  $\Phi^G$  and  $\Theta^G$  on  $m$  and  $G$  in time-switching environments.

Another distinctive feature of  $\Phi^G$  and  $\Theta^G$  is their non-monotonic  $\nu$ -dependence when the other parameters ( $s, m, K_{\pm}, \Omega$ ) are kept fixed. In particular, Fig. 4 shows that  $\Phi^G$  may exhibit a sharp peak in the regime of intermediate  $\nu \in [10^{-4}, 10^{-1}]$  that is well captured by Eq. (24). These results are in marked contrast with their counterparts in a single deme, which vary monotonically with  $\nu$  [16, 17, 19]. The non-monotonic  $\nu$ -dependence  $\Phi^G$  and  $\Theta^G$  is therefore an inherent effect of spatial migration. Intuitively, this behaviour stems, on the one hand, from more  $M$  invasions occurring when the deme size is as close as possible to  $n \approx K_+$ , see Eq. (19). On the other hand, the average deme size is a decreasing function of  $\nu$  [16–18], see Appendix A 2. Therefore, optimising the probability of  $M$  fixation requires two considerations: the environment should avoid remaining stuck in the harsh environment for too long, which can happen with a probability close to 1/2 when  $\nu \ll 1$ ; and the environment should not switch too frequently (i.e.  $\nu \gg 1$ ), as this reduces the effective deme size ( $n \approx \mathcal{K}$ ), which can be significantly smaller than  $K_+$ . Hence, the best conditions for the fixation of  $M$  are for a range of  $\nu$  in the intermediate regime. Since the uMFT is longer in the harsh than in the mild environment (where there are fewer migration events, see Fig. 2(b)), a similar reasoning leads to a minimum mean fixation time for  $\nu$  in the intermediate regime.

## 2. Strong bottlenecks: $\psi(m, K_-) < 1$

When  $\psi(m, K_-) < 1$ , each deme can undergo strong bottlenecks, see Fig. 3(a) and below. In the harsh environment  $\xi = -1$  ( $K = K_-$ ), the entire metapopulation experiences extinction, in an observable time  $\theta_E(K_-, \Omega)$ , denoted  $\theta_E$  here for conciseness. However, in the mild state  $\xi = 1$  ( $K = K_+$ ), deme extinction can be neglected and each site can be regarded as being occupied by either  $W$  or  $M$  cells. The dynamics in the harsh state is thus dominated by extinction, whereas the  $M/W$  competition characterising the mild state is aptly captured by the two-state coarse-grained description of Section III 1. Environmental switching thus couples regimes that are dominated in turn by deme extinction and  $M/W$  compe-

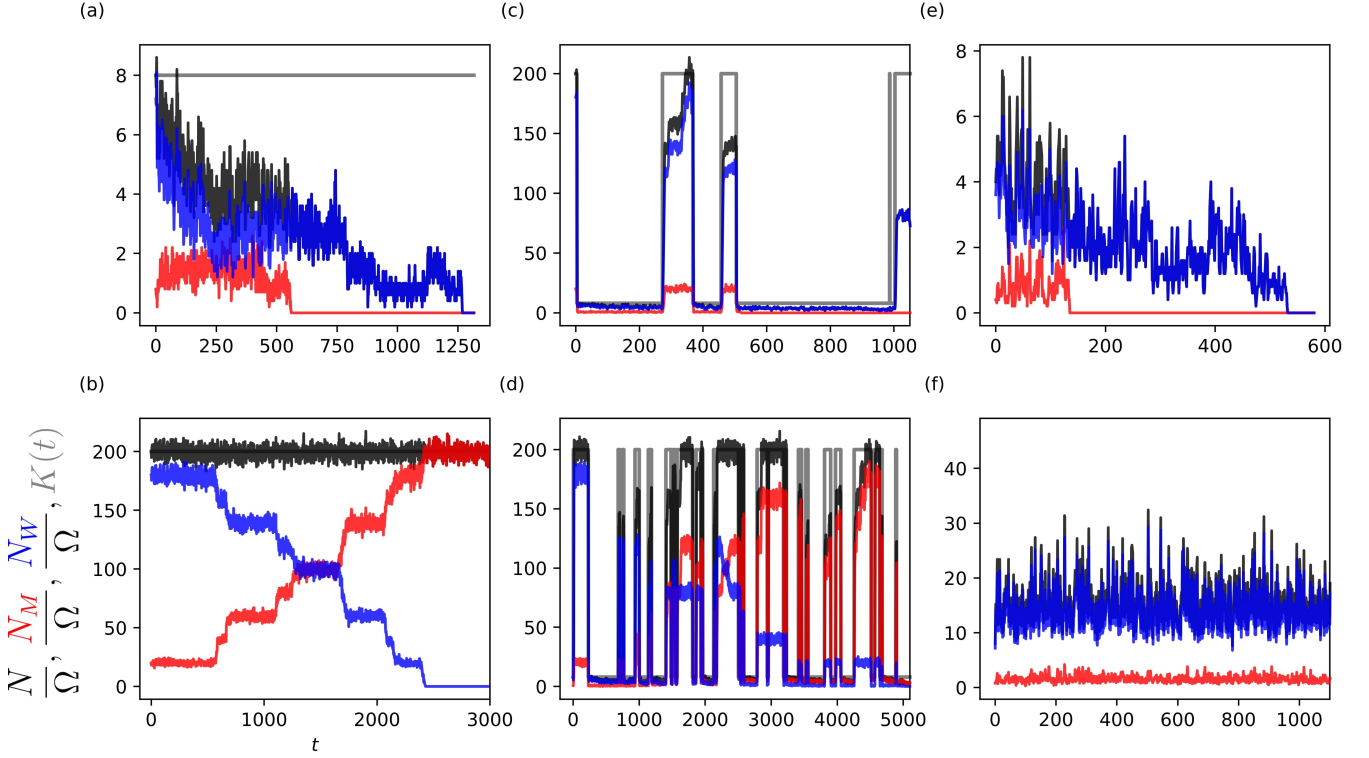


FIG. 5. Typical single realisations of  $N/\Omega$  (black),  $N_M/\Omega$  (red),  $N_W/\Omega$  (blue), and  $K(t)$  (grey) vs time for different values of  $K_-$  and  $\nu$ . (a,b): Here,  $\nu = 10^{-4}$  and  $K_- = 8$ . In (a),  $K = K_-$  at  $t = 0$  and  $M$  and then  $W$  quickly go extinct. In (b),  $K = K_+$  at  $t = 0$  and  $M$  fixes the population while  $W$  goes extinct. (c,d): Here,  $\nu = 10^{-2}$  and  $K_- = 8$ . In (c), mutants survive the first few bottlenecks but their abundance is low leading to the fixation of  $W$  and removal of  $M$  after four bottlenecks ( $t \gtrsim 1000$ ). In (d), mutants survive the first bottlenecks and spread in the mild state where they recolonise and invade demes. They are eventually able to fix the population. (e,f): Here,  $\nu = 10$ , and  $K_- = 4$  in (e) and  $K_- = 10$  in (f).  $K(t)$  switches very frequently and is not shown for clarity. In (e), the deme size is  $n \approx 2K_- = 8$  and the dynamics is dominated by deme extinction leading to the rapid extinction of the metapopulation. In (e), the deme size is  $n \approx 2K_- = 20$  and there is  $M/W$  competition that leads to fixation of  $M$  and extinction of  $W$  after a typical time  $t \sim \theta^{\text{clique}}(2K_-) \gtrsim 10^4$  (not shown). Similar results are obtained on other regular graphs  $G$ , see text. Other parameters are  $\Omega = 10$ ,  $s = 0.1$ ,  $m = 10^{-4}$ , and  $K_+ = 200$ . In all panels, initially there is a single  $M$  deme and  $\Omega - 1$  demes occupied by  $W$ .

tion, yielding complex dynamical scenarios whose analysis is difficult. However, we can gain valuable insight by considering first the limits  $\nu \ll 1$ ,  $\nu \gg 1$ , and then the case of intermediate switching.

When the environment varies very slowly,  $\nu \ll 1$ , the  $K(t)$  remains at its initial value for long periods, that is  $K = K_{\pm}$  if  $\xi(0) = \pm 1$  each with a probability  $1/2$ . On the one hand, if initially  $\xi = -1$  (harsh environment),  $K = K_-$  and each deme is prone to extinction after a mean time  $\tau_E(K_-)$ , which eventually leads to the collapse of the metapopulation after a mMET  $\theta_E \approx e^{K_-} \ln(\Omega)/K_-$  when  $\Omega \gg 1$  and  $K_- \gg 1$ , see Eqs. (6) and (13) and Fig. 5(a). On the other hand, if initially  $\xi = 1$  (mild condition),  $n \approx K_+$  and there is  $M/W$  competition characterised by the fixation of  $M$  with a probability  $\phi(K_+)$  approaching 1 when  $K_+s \gg 1$ , see Eq. (12) and Fig. 5(b). As a result, when  $\nu \ll 1$  and  $K_+s \gg 1$ , there are two equally likely outcomes illustrated in Fig. 5: either the extinction of the metapopu-

lation in a mean time  $\theta_E$  as in Fig. 5(a), or the fixation of  $M$  after a mean time  $\theta^G(K_+)$  as in Fig. 5(b).

In frequently varying environments, when  $\nu \gg 1$ , the size of each deme readily settles about the effective carrying capacity Eq. (15), with  $n \approx \mathcal{K}$  after  $t \sim 1$  [16, 17]. Since  $\mathcal{K} \approx 2K_-$  when  $K_+ \gg K_-$ , if  $\psi(m, 2K_-) < 1$  the dynamics is characterised by the extinction of individual demes and then of the entire metapopulation after mean times  $\tau_E(2K_-)$  and  $\theta_E(\Omega, 2K_-)$ , see Fig. 5(e). However, if  $\psi(m, 2K_-) \gg 1$  and  $2K_-s \gg 1$ , the dynamics is characterised by  $M/W$  competition with  $M$  most likely to fix the metapopulation after a mean time  $\theta^G(2K_-)$ , as illustrated by Fig. 5(f).

In slowly and rapidly changing environments, regardless of the spatial structure, the metapopulation subject to strong bottlenecks is therefore always at risk of either complete extinction or of being taken over by mutants.

In the intermediate switching regime,  $\nu \lesssim 1$  with  $\psi(m, K_-) < 1$ , the metapopulation experiences strong

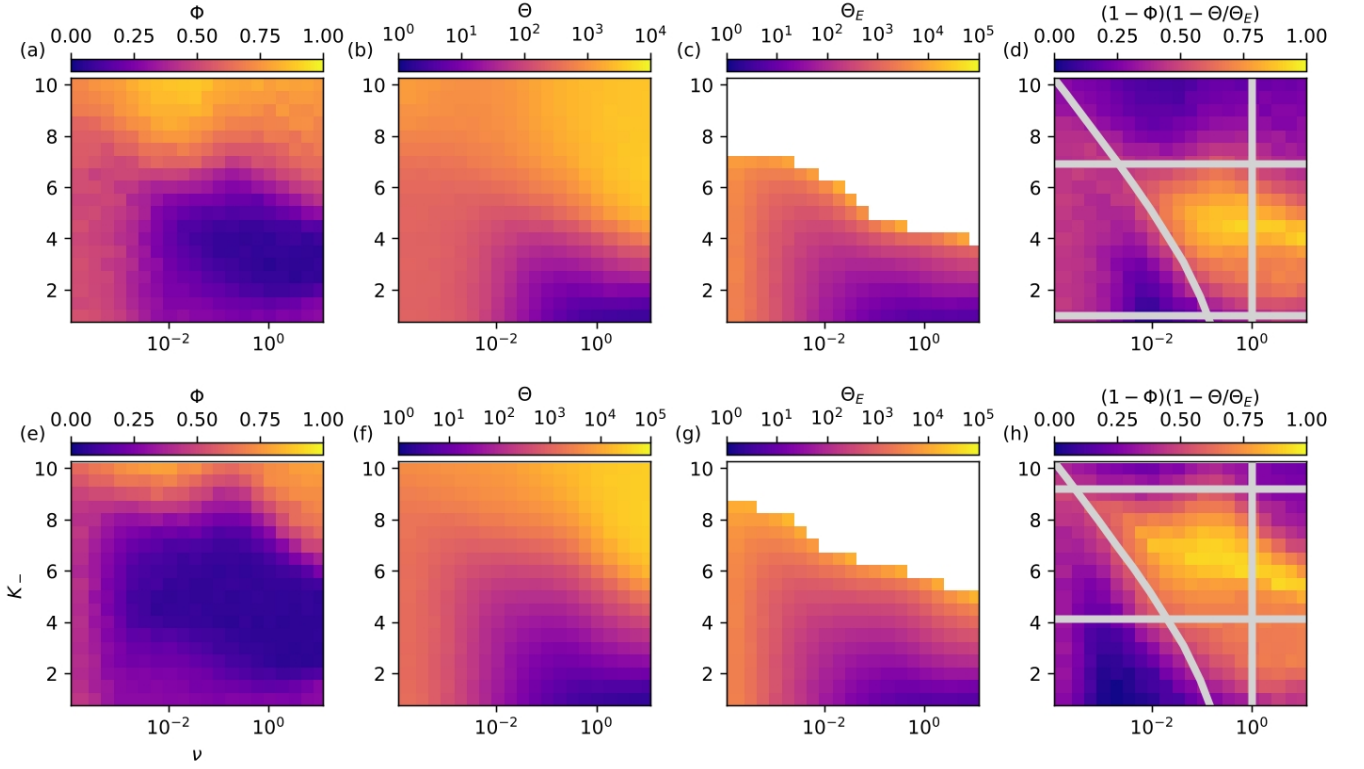


FIG. 6. Near-optimal condition for the idealised treatment.  $(\nu, K_-)$  heatmaps of  $\Phi$ ,  $\Theta$ ,  $\Theta_E$  and  $(1 - \Phi)(1 - \Theta/\Theta_E)$  for a clique metapopulation. The migration rate is  $m = 10^{-3}$  in (a-d) and  $m = 10^{-4}$  in (e-h). Whitespace in panels (c) and (g) indicate where at least one realisation for those parameters did not reach extinction by  $t = 10^5$ , i.e.  $\Theta_E \sim 10^5$  or larger. Grey lines in panels (d) and (h) show the near-optimal conditions for the idealised treatment:  $\psi(m, K_-) < 1$  below the top horizontal line,  $mK_+\theta_E > 1$  above the bottom horizontal line, and  $\nu\theta_E > 1$  above the curved line, while the vertical line indicates where  $\nu < 1$  and  $\theta_E$  from Eq. (13). The near-optimal treatment conditions is the yellowish cloud at the centre of the area enclosed by these lines. Similar results are obtained on other regular graphs  $G$ , see text and Fig. 10. Other parameters  $\Omega = 16$ ,  $s = 0.1$ , and  $K_+ = 200$ . In all panels, initially there is a single  $M$  deme and  $\Omega - 1$  demes occupied by  $W$ .

bottlenecks, can avoid extinction for extended periods of time, and either strain can prevail. In the harsh environmental state ( $K = K_-$ ), the dynamics is always dominated by deme extinction. In the mild state ( $K = K_+ \gg K_-$ ), there is recolonisation of empty demes that rapidly become either  $W$  or  $M$  demes, followed by invasions and  $M/W$  competition. In order to ensure that the collapse of the metapopulation is unlikely to be observed, the mean time spent in either environmental state needs to be shorter than the metapopulation mean extinction time in the harsh environment, i.e.  $1/\nu < \theta_E$ . Moreover, when  $\nu \sim 1/\tau_E(K_-) > 1/\theta_E$ , numerous demes go extinct in the harsh environment before switching to the mild state. Hence, when  $\nu \lesssim 1$  and  $\nu\theta_E > 1$ , the metapopulation is unlikely to go extinct and transiently consists of a mixture of empty demes and  $W/M$  demes before either  $W$  or  $M$  eventually takes over. In this regime, mutants are likely to be removed from the metapopulation when there is a small fraction of them in the harsh environment, see Fig. 5(c). At each strong bottleneck,  $M$  demes have a finite probability to go ex-

tinct before switching to the mild environment, where surviving mutants can invade  $W$  demes and recolonise empty demes. In a scenario illustrated by Fig. 5(c), there are periods of duration  $\sim 1/\nu$  during which the number of mutants remains low and prone to extinction when  $K = K_-$ , followed by periods in  $K_+$  where the number of  $M$  demes increases (due to  $M/W$  competition). Each bottleneck can thus be regarded as an attempt to remove  $M$  demes, whereas each switch  $K_- \rightarrow K_+$  can be envisioned as a rescue of mutants. This cycle repeats itself until  $M$  demes are entirely removed after enough bottlenecks. The metapopulation thus consists of a fluctuating number of  $W$  demes and empty demes. This scenario is the most likely to occur when the initial fraction of  $M$  demes is small. Another possible outcome, illustrated by Fig. 5(d), occurs when mutants surviving the harsh conditions invade and are successful in recolonising many demes in the mild environment. Mutants can thus significantly increase the number of  $M$  demes, exceeding that of  $W$  demes. In this case, bottlenecks can be seen as attempt to remove  $W$  and  $M$  demes, and the most likely

outcome is the removal of  $W$  demes. In this scenario, the metapopulation eventually consists of a fluctuating number of empty demes and mutant demes, as illustrated by Fig. 5(d). The results of Fig. 5 have been obtained for cliques, but the same qualitative behaviour is expected for any regular graphs  $G$ , with the spatial structure affecting the the long-term fraction of occupied demes and therefore the probability of removal of each bottleneck. However, phenomena operated by extinction are mostly independent of  $G$  and  $m$ , as illustrated by Fig. 10.

*A hypothetical idealised treatment:* In this intermediate switching regime, the metapopulation is likely to avoid extinction in the harsh environment if  $\nu\theta_E \gtrsim 1$ . Moreover, when  $mK_+\theta_E \gtrsim 1$  enough demes are recolonised in the mild environment to ensure that the metapopulation will not readily go extinct after a bottleneck. Hence, the metapopulation is likely to avoid extinction when  $\nu\theta_E > 1$  and  $mK_+\theta_E > 1$  and either  $W$  or  $M$  can be entirely removed, with respective probabilities  $\Phi$  and  $1 - \Phi$ , after a mean time  $\Theta$ , whereas the mMET in the time-fluctuating environment,  $\Theta_E$ , occurs on a much longer timescale ( $\Theta_E \gg \Theta$ ). As an application, we consider a hypothetical idealised treatment to efficiently remove deleterious mutants from an otherwise healthy system by controlling the environmental conditions via the parameters  $K_-$  and  $\nu$ . In this context,  $M$  cells are interpreted as deleterious mutants that have a selective advantage over healthy  $W$  cells composing an organism, here represented by the metapopulation consisting initially of  $\Omega - 1$  demes of type  $W$  and a single  $M$  deme. Small numbers of pathogenic cells, as few as 10 for some strains of *Salmonella* and *Shigella* [86, 87], can cause illness and so these initial conditions are relevant, even for smaller systems. The idealised treatment consists of finding the set of near-optimal environmental conditions to remove  $M$  cells and minimise the risk of extinction of the entire metapopulation. This corresponds to determining the range of  $K_-$  and  $\nu$  for which  $\Phi$  and  $\Theta/\Theta_E$  are minimal. According to the above discussion, the near-optimal conditions for this idealised treatment on a regular graph  $G$  are

$$\psi(m, K_-) < 1, \quad \nu \lesssim 1, \quad \nu\theta_E \gtrsim 1, \quad mK_+\theta_E \gtrsim 1. \quad (25)$$

Under these conditions, illustrated in Fig. 6, which depend on  $m$  but not on the spatial structure  $G$ , environmental variability generates a succession of strong bottlenecks at a frequency ensuring that the mutant type is the most likely to go extinct in a mean time that is much shorter than the metapopulation mean extinction time. While determining analytically  $\Phi$  and  $\Theta/\Theta_E$  satisfying Eq. (25) is challenging, this can be done efficiently numerically as illustrated by the heatmaps of Fig. 6, and be summarised by maximising the composite quantity  $(1 - \Phi)(1 - \Theta/\Theta_E)$ , as shown in Fig. 6(d,h). In the examples of Fig. 6, we find that the near-optimal treatment conditions are  $10^{-2} \lesssim \nu \lesssim 1$  and for  $K_-$  that changes with  $m$ :  $K_- \in [2, 7]$  for  $m = 10^{-3}$  and  $K_- \in [4, 9]$  for  $m = 10^{-4}$ . The idealised treatment therefore consists

of letting the metapopulation evolve under the near optimal conditions Eq. (25), under which it undergoes a series of strong bottlenecks whose expected outcome is the removal of mutants. Once all mutants are removed, as in Fig. 5(c), the final course of the treatment consists of keeping the metapopulation in the mild environment (with  $K = K_+$ ), where  $W$  cells would spread and finally take over all the demes. In the example of Fig. 5(c), this would be achieved by setting  $K = K_+$  after  $t \gtrsim 1000$ . This idealised treatment, illustrated for clique metapopulations in Fig. 6, qualitatively holds on regular graphs  $G$ , with small influence of the spatial structure on the shape of the heatmap when  $m$  is kept fixed, as seen by comparing Figs. 6(e-h) and 10.

## V. DISCUSSION, GENERALISATIONS AND ROBUSTNESS

Here, we discuss our main results by critically reviewing our assumptions and outline possible generalisations. We have studied the eco-evolutionary dynamics of a metapopulation consisting of  $\Omega$  identical demes with the same carrying capacity  $K$ , containing wild-type  $W$  and mutant  $M$  cells, that are connected by slow migration and arranged according to regular circulation graphs. While our approach holds for any regular graph, we have specifically considered the examples of cliques (island model), cycles, and square grids (with periodic boundaries) which are all *circulation* graphs, i.e. the rate of in-flow and out-flow migration is the same at each deme. This has allowed us to consider the effect of both weak and strong local correlations arising respectively in clique and cycle metapopulations. We have analysed the metapopulation dynamics in a static environment where  $K$  is constant, and in a time-varying environment where  $K$  switches endlessly between  $K_+$  and  $K_- < K_+$  at a rate  $\nu$ , see Eq. (5). In static environments, the deme size fluctuates about  $K$  and the metapopulation dynamics is characterised by either  $M/W$  competition (when  $\psi \gg 1$ ), or by deme extinction (when  $\psi < 1$ ). We have used suitable coarse-grained descriptions to analytically characterise the fate of the population in those regimes, see Fig. 2. When, as here, the metapopulation is spatially arranged on circulation graphs, the circulation theorem [41, 47] guarantees that the fixation probability in the competition-dominated regime is independent of the migration rate and the spatial structure. We have also devised a coarse-grained three-state description of the dynamical equilibrium in the crossover regime (where  $\psi \gtrsim 1$ ) where in the long run there is a mixture of occupied demes of type  $W$  or  $M$  and empty demes, see Sec. F. In time-fluctuating environments, when  $K$  switches neither too quickly nor too slowly, each deme is subject to bottlenecks that can be weak when  $K_-$  is large enough to ensure  $\psi(m, K_-) \gg 1$ . Deme extinction can be neglected in the weak bottleneck regime, and we have combined a coarse-grained description with a PDMP approximation

to characterise the  $W/M$  competition in time-varying environments in the absence of deme extinction. This has allowed us to show that weak bottlenecks lead to a *non-monotonic* dependence of the mutant fixation probability  $\Phi^G$  and mean fixation time  $\Theta^G$  on the switching rate  $\nu$ , with an explicit dependence on the migration rate, whereas the spatial structure has an unnoticeable effect on  $\Phi^G$ , regardless of spatial correlations, but influences  $\Theta^G$ . When demes are subject to strong bottlenecks, metapopulation extinction is a likely outcome under slow and fast switching ( $\nu \ll 1$  and  $\nu \gg 1$ ), whereas the overall extinction can be avoided for long periods under intermediate switching, when  $W/M$  competition and deme extinction dynamics are coupled. As a hypothetical application, we have considered an idealised treatment for the rapid removal of the mutant conditioned on minimising the risk of overall extinction.

The coarse-grained descriptions adopted in the static and dynamic environments track the dynamics of a single unbreakable cluster of  $M$  demes ( $M$ -cluster). This requires starting from such a cluster, where here we assumed the natural initial condition of a single  $M$  deme. Other starting configurations are also possible (e.g. two or more neighbouring  $M$  demes) provided that the unbreakable structure of the  $M$ -cluster is preserved at all times  $t \geq 0$ . For the sake of concreteness and simplicity, we have focused on a class of regular circulation graphs. As the number of active edges connecting  $W$  and  $M$  demes in cliques and cycles is known exactly, these graphs are particularly amenable to detailed analysis. In two dimensions, spatial correlations between demes are more complex, and the coarse-grained description of the  $M/W$  competition dynamics on a grid has required approximations of the number of active edges, see Appendix E. A similar approximation is expected to hold on hypercubic lattices (with periodic boundaries). These considerations on the role of the initial condition and spatial structure do not matter when the metapopulation dynamics is dominated by the extinction of demes since these occur randomly. As a consequence, the “idealised treatment” method based on the dynamic coupling of competition and deme extinction to remove a targeted strain is expected to hold on more complex structures, including generic regular graphs.

In this work, we have focused on the biologically relevant regime of slow migration, which is well known to increase the population fragmentation and hence influences its evolution and diversity [61, 88]. Here, the assumption of slow migration is crucial for the coarse-grained description of the metapopulation dynamics, and the values considered in our examples,  $m \approx 10^{-5} - 10^{-2}$  (see Appendix B), are comparable with those used in microfluidic experimental setups [63]. For  $m \gg 1$ , the behaviour of a single well-mixed deme is recovered, see Ref. [16]. For intermediate  $m$ , the dynamics is characterised by coarsening, i.e. the slow growth of domain sizes over time [89, 90]. For the sake of simplicity and without loss of generality, we have assumed that migra-

tion occurs without any directional preference and with the same rate for  $M$  and  $W$ . These assumptions can be relaxed and the coarse-grained description be readily generalised to the case of directional and type-specific migration [51], yielding the same qualitative behaviour discussed here for circulation graphs. We note however that asymmetric directional migration significantly affects the evolutionary dynamics on non-circulation graphs, like the star [41, 42, 50, 54]. It would be interesting to study the evolution on these non-circulation graphs in time-varying environments in the case of symmetric and directional migration. For computational tractability, we have chiefly considered metapopulations consisting of 16 demes of size ranging between 1 and 200, which are much smaller systems than most realistic microbial communities. However, we note that with microfluidic devices and single-cell techniques, it is possible to perform spatially structured experiments with 10 to 100 cells per microhabitat patch, which are conditions close to those used in our model [63, 91, 92]. Moreover, *in-vivo* host-associated metapopulations are often fragmented into a limited number of relatively small demes, e.g.  $\Omega \approx 25$  and  $K \approx 1000$  in mouse lymph nodes [60, 93, 94].

Here, we have conveniently represented environmental variability by the random switching of the carrying capacity  $K = \{K_+, K_-\}$  driven by a symmetric dichotomous Markov noise (DMN), with the extension to asymmetric DMN outlined in Appendix H. DMN is commonly used to model evolutionary processes because it is simple to simulate and analyse, and closely reproduces the binary conditions used in many laboratory-controlled experiments. These are typically carried out in periodically changing environments [79, 95, 96]. It has however been shown that letting  $K$  vary periodically between  $K_+$  and  $K_-$  with a period  $1/(2\nu)$  leads to essentially the same dynamics [18]. Moreover, the relationship between DMN used here and other common forms of environmental noise has been extensively studied [18, 19, 69, 70], showing that DMN is a convenient and non-limiting choice to model environmental variability.

## VI. CONCLUSIONS

Cells evolve in spatially structured settings, where the competition with those nearby is stronger than those further afield, subject to never-ending environmental changes. Spatial structure and environmental variability impact the eco-evolutionary dynamics of microbial populations significantly, but their joint influence is scarcely considered. Mutations frequently arise in cell communities and some may have deleterious effects, e.g. causing the rise of resistance to antibiotics [21, 30–32]. Motivated by these issues, and inspired by recent advances in microfluidics allowing experiments to track dynamics at the single-cell level [63, 91, 92], we have investigated the prototypical example of a rare mutant having a selective advantage over wild-type resident cells occupying a



spatially structured population in time-fluctuating environments. Here, we have considered a class of metapopulation models spatially arranged as regular (circulation) graphs where cells of wild and mutant types compete in a *time-fluctuating* environment. The metapopulation consists of demes (subpopulations) with the same carrying capacity, connected to each other by slow cell migration. We represent environmental variability by letting the carrying capacity endlessly switch between two values associated to harsh and mild conditions. In this framework, we have studied how migration, spatial structure, and fluctuations influence the probability and time for the mutant or wild-type to take over the metapopulation, and under which conditions extinction of demes and the entire metapopulation occurs. This allows us to identify when environmental variability coupled to demographic fluctuations can be utilised to remove the mutant.

We have first considered the case where demes fluctuate about a constant carrying capacity in static environments. We have thus characterised analytically and using stochastic simulations a regime dominated by the competition between the mutants and wild-type cells, another one where there is deme extinction, as well as a crossover regime combining local competition and extinction. In time-varying environments, various qualitatively different dynamical scenarios arise and environmental fluctuations can significantly influence the evolution of metapopulations. When the rate of switching is neither too slow nor too fast, demes experience bottlenecks and the population is prone to fluctuations or extinction. When the fluctuating carrying capacity remains large and bottlenecks are weak, deme extinction is negligible. The dynamics is thus dominated by the competition between wild-type cells and mutants to invade and take over demes, and eventually the population, which we characterise by devising a suitable coarse-grained description of the individual-based model when migration is slow. This allows us to determine the fixation probability and mean fixation time by combining analytical and computational tools, and to show that these quantities can vary non-monotonically with the environmental switching rate. We find that in the regime of weak bottlenecks, the mutant fixation probability on regular circulation graphs depends on the migration rate, which is in stark contrast with what happens in static environments, while the spatial structure has no noticeable influence. When the carrying capacity is small under harsh conditions, bottlenecks are strong and there is a dynamical coupling of strain competition in the mild environmental state and deme extinction in the harsh environment. This yields rich dynamical scenarios among which we identify a mechanism, expected to hold on any regular graph, driven by environmental variability and fluctuations to efficiently eradicate one strain. As a hypothetical application, we have thus proposed an idealised treatment to remove the mutant, assumed to be deleterious and favoured by selection. We have shown that when each deme is subject to strong bottlenecks at a certain

intermediate switching rate the mutant can be efficiently removed by demographic fluctuations arising in the harsh environment without exposing the entire population to a risk of rapid extinction. We have thus determined the near-optimal conditions on the switching rate and bottleneck strength for this idealised treatment and found that these are qualitatively the same on other graphs.

In summary, our analysis sheds further light on the influence of the spatial structure, migration, and fluctuations on the spread of a mutant strain in time-fluctuating environments. We have identified and characterised various dynamical scenarios, displaying a complex dependence on the switching and migration rates. We have also shown how environmental variability and fluctuations can be utilised to achieve desired evolutionary outcomes like the efficient removal of a deleterious mutant. While we have made a number of simplifying assumptions, allowing us to make analytical progress, many of these can be relaxed without affecting the results or the methodology. Our approach holds for arbitrary regular graphs and can be generalised to more complex spatial settings. We therefore believe that the model studied here has numerous potential applications. For instance, it mirrors the *in vitro* evolution of a mutant across an array of microfluidic devices, where cells migrate between “microhabitat patches” either via microchannels or pipette, with bottlenecks implemented via a strict control of the nutrient level in each device.

**Data availability statement:** The data and codes that support the findings of this study are openly available at the following URL/DOI: 10.5518/1660 [97].

## ACKNOWLEDGMENTS

We would like to thank K. Distefano, L. Hernández-Navarro, J. Jiménez, S. Muñoz-Montero, M. Pleimling, and A. M. Rucklidge for fruitful discussions. M. M. gratefully acknowledges funding from the U.K. Engineering and Physical Sciences Research Council (EPSRC) under the Grant No. EP/V014439/1 for the project ‘DMS-EPSRC Eco-Evolutionary Dynamics of Fluctuating Populations’. The support of a Ph.D. scholarship to M. A. by the EPSRC Grant No. EP/T517860/1 is also thankfully acknowledged. M. S. and U. C. T.’s contribution to this research was supported by the U.S. National Science Foundation, Division of Mathematical Sciences under Award No. NSF DMS-2128587. This work was undertaken on ARC4, part of the High Performance Computing facilities at the University of Leeds, UK.

## Author contributions

**Matthew Asker:** Conceptualisation (supporting), Formal analysis, Data curation, Investigation, Methodology, Software, Validation, Visualisation, Writing – orig-

inal draft, Writing – review & editing. **Mohamed Swailem**: Conceptualisation (supporting), Formal analysis, Data curation, Investigation, Software, Validation, Writing – review & editing. **Uwe C. Täuber**: Funding acquisition, Supervision, Resources, Writing – review & editing. **Mauro Mobilia**: Conceptualisation, Formal analysis, Methodology, Validation, Funding acquisition, Supervision, Resources, Writing – original draft, Writing – review & editing.

### Appendix A: Further details on the model

In this section, we provide further details on the model by discussing the master equation encoding its individual-based dynamics, and give further details of the size distribution of a single deme.

### 1. Master equation

As discussed in Sec. II, the individual-based model is a continuous-time multivariate Markov process defined by the reaction and transition rates Eq. (1)-(4). The intra and inter-deme dynamics is encoded in a master equation for the probability  $P(\{n_W, n_M\}, \xi, t)$  that at time  $t$  the metapopulation is in the environmental state  $\xi$  and configuration  $\{n_W, n_M\} \equiv (\dots, n_W(x), n_M(x), \dots)$ , where  $n_{W/M}(x)$  denotes the number of cells of type  $W/M$  in deme  $x = 1, \dots, \Omega$ . The master equation (ME) for the metapopulation dynamics subject to environmental switching on a regular graph  $G = \{\text{clique, cycle, grid}\}$  of degree (or number of nearest neighbours)

$$q_G = \begin{cases} \Omega - 1, & G = \text{clique} \\ 2, & G = \text{cycle} \\ 4, & G = \text{grid}, \end{cases} \quad (\text{A1})$$

reads:

$$\begin{aligned} \frac{\partial P(\{n_W, n_M\}, \xi, t)}{\partial t} &= \sum_{x=1}^{\Omega} \sum_{\alpha} [(\mathbb{E}_{\alpha}^{-}(x) - 1) T_{\alpha}^{-}(x) P(\{n_W, n_M\}, \xi, t) + (\mathbb{E}_{\alpha}^{+}(x) - 1) T_{\alpha}^{+}(x) P(\{n_W, n_M\}, \xi, t)] \\ &+ \frac{1}{2} \sum_{x=1}^{\Omega} \sum_{y \text{ n.n. } x} [(\mathbb{E}_W^{+}(y) \mathbb{E}_W^{-}(x) - 1) T_W^{m,G}(x) + (\mathbb{E}_W^{+}(x) \mathbb{E}_W^{-}(y) - 1) T_W^{m,G}(y)] P(\{n_W, n_M\}, \xi, t) \\ &+ \frac{1}{2} \sum_{x=1}^{\Omega} \sum_{y \text{ n.n. } x} [(\mathbb{E}_M^{+}(y) \mathbb{E}_M^{-}(x) - 1) T_M^{m,G}(x) + (\mathbb{E}_M^{+}(x) \mathbb{E}_M^{-}(y) - 1) T_M^{m,G}(y)] P(\{n_W, n_M\}, \xi, t) \\ &+ \nu [P(\{n_W, n_M\}, -\xi, t) - P(\{n_W, n_M\}, \xi, t)], \end{aligned} \quad (\text{A2})$$

where  $y \text{ n.n. } x$  denotes the sum over the  $q_G$  neighbours  $y$  of the deme  $x$  and  $P(\dots) = 0$  whenever any of  $T_{\alpha}^{\pm}$  or  $T_{\alpha}^{m,G}$  is negative. The shift operators  $\mathbb{E}_{\alpha}^{\pm}(x)$  act by raising or decreasing by one the number of cells of type  $\alpha$  in deme  $x$ . For example,  $\mathbb{E}_W^{\pm}(x)[n_W(x)P(\dots, n_W(x), n_M(x), \dots, \xi, t)] = (n_W(x) \pm 1)P(\dots, n_W(x) \pm 1, n_M(x), \dots, \xi, t)$  and  $\mathbb{E}_M^{\pm}(x)[n_W(x)P(\dots, n_W(x), n_M(x), \dots, \xi, t)] = n_W(x)P(\dots, n_W(x), n_M(x) \pm 1, \dots, \xi, t)$ . The first line on the right-hand-side (RHS) of Eq. (A2) encodes the inter-deme birth-death dynamics, the second and third lines represent the intra-dynamics via inward and outward migration, and the last line accounts for symmetric random environmental switching. Here, the ME has specifically been formulated in the presence of environmental switching, but its static-environment counterpart is readily obtained from A2: it suffices to set  $\nu = 0$  and to replace  $K(t)$  by a constant carrying capacity  $K$ , yielding the ME for  $P(\{n_W, n_M\}, t)$  that is the probability to find the metapopulation in a given state  $\{n_W, n_M\}$  at time  $t$  (with no environmental dependence). Moreover, by setting  $\Omega = 1$  and  $m = 0$  in

Eq. (A2), the second and third lines on the RHS cancel, we obtain the ME encoding the inter-deme dynamics of a single isolated deme [16, 17].

While the ME Eq. (A2) holds for any regular graphs  $G$ , in our examples we consider specifically the regular circulation graphs  $G = \{\text{clique, cycle, grid}\}$ . The space-dependent individual-based dynamics encoded in the ME Eq. (A2) has been simulated using the Monte Carlo method described in Section I. It is worth noting that demographic fluctuations eventually lead to the extinction of the entire metapopulation, in all regimes. However, this phenomenon occurs after a time growing dramatically with the system size, and it can generally not be observed in sufficiently large metapopulations, see Fig. 2(f,g).

### 2. Eco-evolutionary dynamics of a single deme

Since the metapopulation consists of a graph of connected demes, all with the same carrying capacity, we can gain significant insight into its dynamics by looking

into its building block. In this section, we therefore analyse the eco-evolutionary dynamics of single isolated deme (when  $m = 0$ ).

For an isolated deme, there is only intra-deme dynamics according to the birth-death process defined by Eqs. (1) and (2). The ME for the dynamics of a single isolated deme is thus given by setting  $\Omega = 1$  and  $m = 0$  in Eq. (A2), see Appendix A 1. The corresponding intra-deme dynamics in a time-varying environment can thus be simulated using exact methods like the Gillespie algorithm [98], as in Refs [16–18, 20–24]. It is instructive to ignore all forms of fluctuations and consider the mean-field approximation of an isolated deme dynamics subject to a constant carrying capacity  $K \gg 1$ . Following Refs. [16, 17], with the transition rates Eq. (2), the mean-field eco-evolutionary dynamics of a single isolated deme is characterised by rate equations for the size  $n$  of the deme and the fraction  $x = n_M/n$  of mutants in the deme, which read:

$$\begin{aligned} \dot{n} &= \sum_{\alpha} T_{\alpha}^{+} - \sum_{\alpha} T_{\alpha}^{-} = n \left(1 - \frac{n}{K}\right), \\ \dot{x} &= \frac{T_M^{+} - T_M^{-}}{n} - x \frac{\dot{n}}{n} = \frac{sx(1-x)}{1+sx}, \end{aligned} \quad (\text{A3})$$

where the dot indicates the time derivative and we have used  $f_M = 1 + s$  and  $f_W = 1$ . These decoupled rate equations predict the quick relaxation of the deme size towards the constant carrying capacity, with  $n \rightarrow K$  on a timescale  $t \sim 1$ , and the growth of the fraction of mutants, with  $x \rightarrow 1$  on a timescale  $t \sim 1/s$ . In the total absence of fluctuations, when  $0 < s \ll 1$  (small selective advantage to  $M$ ), in the mean-field picture, the deme size quickly approaches the carrying capacity and there is a timescale separation between  $n$  and  $x$ , respectively the fast and slow variables.  $W$  cells are thus slowly wiped out by mutants that take over the deme on a timescale  $t \sim 1/s \gg 1$  [16, 17]. It is worth noting that with the effective transition rates Eq. (19) we have assumed that invasions always occur after deme size and composition relaxation. This means that Eqs. (23) and (24) assume a timescale separation between  $n$  and  $x$  and  $x$  and the number of  $M$  demes.

It is also relevant to consider the intra-deme dynamics of a single isolated site subject to a finite constant carrying capacity  $K$ . As explained in Appendix B, the intra-deme dynamics can be well approximated by a Moran process for a deme of constant size  $n = K$  [7, 16, 17, 64–66], and characterised by the fixation probability and mean fixation time given by Eq. (B3). The probability  $\rho_{M/W}(K)$  that a single  $M/W$  cell takes over a  $W/M$  deme of size  $K$  is given by Eq. (9).

When demographic fluctuations can be neglected and randomness only arises from environmental variability via Eq. (5), the intra-deme dynamics of an isolated deme is well-captured by the piecewise deterministic Markov process (PDMP) for  $n$ , obtained by ignoring demographic fluctuations [16, 17, 84]. In the realm of the PDMP approximation, the deme size thus satisfies a deterministic

logistic equation in each environmental state, subject to a carrying capacity that switches when the environment changes ( $K = K_{\pm}$  when  $\xi = \pm 1$ ), yielding the following  $n$ -PDMP [16–18, 21, 22, 32]:

$$\dot{n} = \begin{cases} n \left(1 - \frac{n}{K_{-}}\right) & \text{if } \xi = -1, \\ n \left(1 - \frac{n}{K_{+}}\right) & \text{if } \xi = 1, \end{cases} \quad (\text{A4})$$

that is decoupled from the mean-field equation for  $x$  that is as in Eq. (A3). The stationary joint probability density of this  $n$ -PDMP is given by Eq. (17) [17, 18], while the marginal probability density is

$$p(\nu, n) = \frac{1}{2} \sum_{\xi} p_{\xi}(\nu, n) = \frac{\mathcal{Z}}{n^2} \left[ \left( \frac{K_{+}}{n} - 1 \right) \left( 1 - \frac{K_{-}}{n} \right) \right]^{\nu-1}, \quad (\text{A5})$$

where  $\mathcal{Z}$  is the normalisation constant and  $n \in [K_{-}, K_{+}]$ . Despite ignoring the effect of demographic noise,  $p(\nu, n)$  aptly captures many properties of the quasi-stationary distribution of the size of an isolated single deme [17, 18]. For instance, the long-time average deme size is accurately approximated by  $\mathcal{N}(\nu) = \int_{K_{-}}^{K_{+}} np(\nu, n)dn$ , and is a decreasing function of  $\nu$  [16, 17]. As illustrated by Fig. 7, the density  $p(\nu, n)$  correctly predicts that the deme size distribution is bimodal when  $\nu < 1$  and unimodal when  $\nu > 1$ , and that it is peaked at  $n \approx K_{\pm}$  when  $\nu \ll 1$  (slow switching) and centred around  $n \approx \mathcal{K}$  when  $\nu \gg 1$  (fast switching), see Eq. (15). The joint and marginal PDMP probability densities Eq. (17) and Eq. (A5) provide valuable insight into the deme size distribution when these are subject to weak bottlenecks and their extinction can be neglected [16–19, 21, 22, 32].

While  $p_{\xi}(\nu, n)$  and  $p(\nu, n)$  give a PDMP description of the quasi-stationary distribution of the size of an isolated deme ( $m = 0$ ), the  $n$ -PDMP stationary densities (17) and (A5) are still a valid approximations of the long-time size distribution of  $n$  in the presence of migration as considered here. In fact, as shown below in Fig. 7, the influence of migration on the distribution of the deme size is essentially unnoticeable, and its main features are therefore well captured by Eq. (17) and Eq. (A5).

In the main text, we have used the PDMP approximation to describe the size distribution of a single isolated deme subject to symmetric random switching of its carrying capacity Eq. (5). Here, we show that spatial migration has no noticeable influence on the size distribution of a single deme of a metapopulation structured as a regular circulation graph  $G = \{\text{clique, cycle, grid}\}$ . To this end, in Fig. 7, we compare the size distribution of a single deme in a metapopulation structured as a regular  $G$ -graph in the presence of a migration per capita rate  $m = 10^{-3}$  (obtained from stochastic simulations) with the predictions of Eq. (17). These results illustrate that migration has no noticeable effect on the deme size distribution that can be approximated by PDMP density Eq. (17) (or Eq. (A5)) in the absence and presence of migration on any graph  $G = \{\text{clique, cycle, grid}\}$

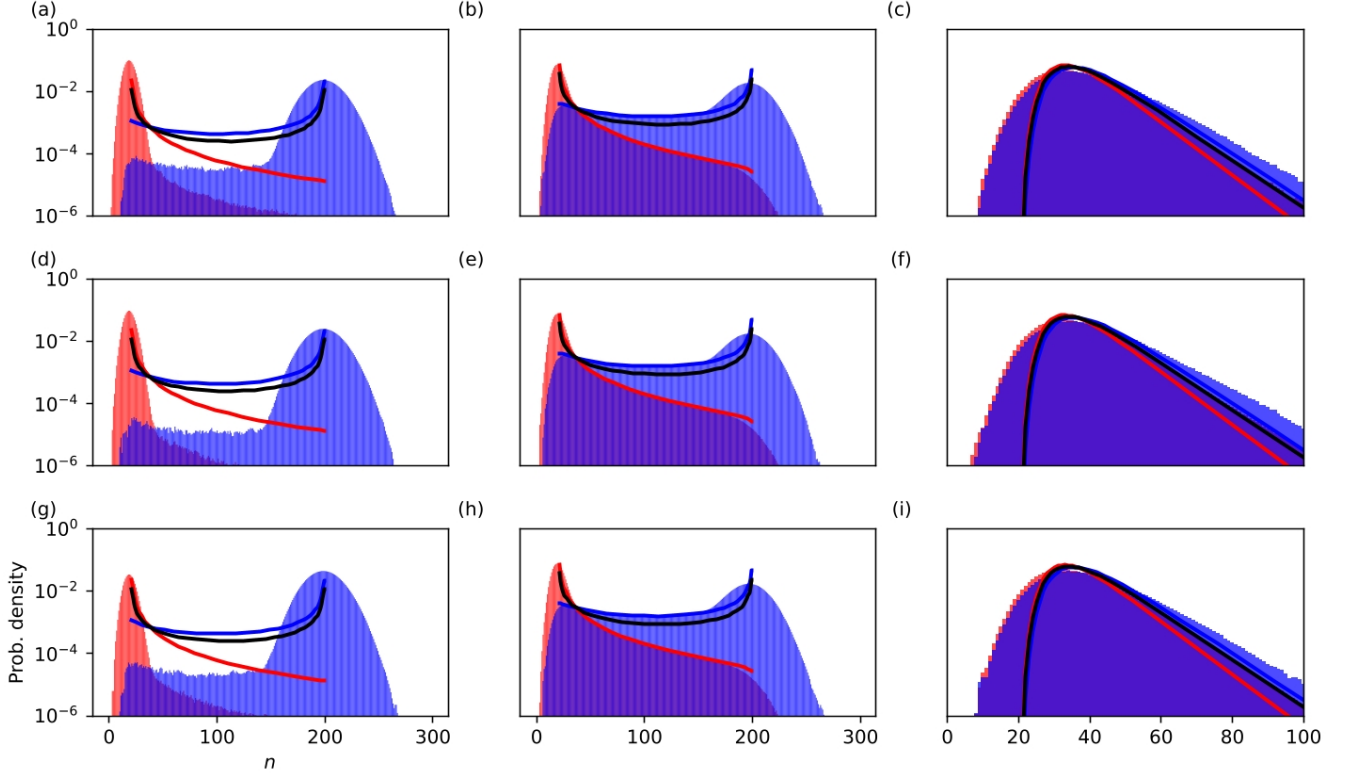


FIG. 7. Quasi-stationary probability density of deme population size ( $n$ -QPD) distribution for various parameters and its  $n$ -PDMP approximation by (17) and (A5). Red and blue bars show data for the  $n$ -QPD conditioned on  $K(t) = K_-$  and  $K(t) = K_+$ , respectively. Red, blue, and black solid lines are the  $n$ -PDMP stationary densities  $p_-(\nu, n)$ ,  $p_+(\nu, n)$ , and  $p(\nu, n)$ , respectively, given by Eqs. (17) and (A5). (a-c) are for clique, (d-f) for cycle, and (g-i) for grid metapopulations. We have  $\nu = 10^{-3}$  in (a,d,g),  $\nu = 10^{-1}$  in (b,e,h), and  $\nu = 10^2$  in (c,f,i). Other parameters are  $\Omega = 16$ ,  $m = 10^{-3}$ ,  $K_+ = 200$ , and  $K_- = 20$ . All represent a single realisation tracked until  $t = 10^5$ .

As a consequence, the deme size distribution of any metapopulation considered here is well approximated by the joint and marginal PDMP densities  $p(\pm, \nu, n)$  and  $p(\nu, n)$ , given by Eq. (17) and Eq. (A5).

Intuitively, this can be understood by noticing that the spatial structures considered here are circulation graphs, yielding the same inward and outward migration flow at each deme, and each deme has the same carrying capacity. As a consequence, the average number of cells per deme is expected to be independent of migration. The latter remains well captured by  $p(\pm, \nu, n)$  and  $p(\nu, n)$  on all spatial structures considered here, as seen in Fig. 7.

## Appendix B: Deme invasion and slow migration

In this section, we analyse the process of invasion of a single deme subject to a constant carrying capacity  $K$  when  $\psi(m, K) \gg 1$ , see Sec. III 1. In this competition-dominated regime, the extinction of demes can be neglected and their size rapidly fluctuated about  $K$ , see Fig. 1(a). In this scenario, we can assume that the deme size is constant  $n(x) = K$ , and describe the deme dy-

namics by tracking the number of mutants  $n_M$  and wild-type cells  $n_W$  in the deme  $x$ . The deme composition  $(n_M, n_W) = (n_M, K - n_M)$  thus changes according to the Moran process [7, 64–66]

$$\begin{aligned} (n_M, n_W) &\xrightarrow{\mathcal{T}_{M\Omega}^+} (n_M + 1, n_W - 1), \\ (n_M, n_W) &\xrightarrow{\mathcal{T}_{M\Omega}^-} (n_M - 1, n_W + 1), \end{aligned} \quad (\text{B1})$$

where the transition rates are defined in terms of  $T_{M/W}^\pm$ , given by Eq. (2), according to [16, 17, 21, 22]

$$\begin{aligned} \mathcal{T}_{\text{Mo}}^+(n_M) &= \frac{T_M^+ T_W^-}{K} = \frac{f_M}{f} \frac{n_M n_W}{K} = \frac{f_M}{f} n_M \left(1 - \frac{n_M}{K}\right), \\ \mathcal{T}_{\text{Mo}}^-(n_M) &= \frac{T_M^- T_W^+}{K} = \frac{f_W}{f} \frac{n_M n_W}{K} = \frac{f_W}{f} n_M \left(1 - \frac{n_M}{K}\right). \end{aligned} \quad (\text{B2})$$

These transition rates correspond to the effective rates of increase and decrease in the number of  $M$  in a deme of size  $K$ . This Moran process conserves the deme size by accompanying each birth of an  $M/W$  by the simultaneous death of a  $W/M$ , and is characterised by

the absorbing states  $(n_M, n_W) = (K, 0)$  ( $M$  deme) and  $(n_M, n_W) = (0, K)$  ( $W$  deme). The  $M$  fixation probability  $\phi_{\text{Mo}}$  and unconditional mean fixation time (uMFT)  $\theta_{\text{Mo}}$  for this Moran process are classical results, and when there are initially  $i$  cells of type  $M$ , they read [7, 65–67]

$$\begin{aligned}\phi_{\text{Mo}}(i) &= \frac{1 - \gamma_{\text{Mo}}^i}{1 - \gamma_{\text{Mo}}^K}, \\ \theta_{\text{Mo}}(i) &= \phi_{\text{Mo}}(i) \sum_{n=i}^{K-1} \sum_{l=1}^n \frac{\gamma_{\text{Mo}}^{n-l}}{\mathcal{T}_{\text{Mo}}^+(l)} \\ &\quad - (1 - \phi_{\text{Mo}}(i)) \sum_{n=1}^{i-1} \sum_{l=1}^n \frac{\gamma_{\text{Mo}}^{n-l}}{\mathcal{T}_{\text{Mo}}^+(l)},\end{aligned}\quad (\text{B3})$$

where  $\gamma_{\text{Mo}} \equiv \mathcal{T}_{\text{Mo}}^-/\mathcal{T}_{\text{Mo}}^+ = f_W/f_M = 1/(1+s)$ . The fixation probability of a single mutant ( $i=1$ ) and of a single  $W$  cell ( $i=K-1$ ) are particularly relevant for our purposes, and explicitly read

$$\begin{aligned}\rho_M \equiv \phi_{\text{Mo}}(1) &= \frac{s}{1+s} \left[ \frac{1}{1 - (1+s)^{-K}} \right], \\ \rho_W \equiv 1 - \phi_{\text{Mo}}(K-1) &= \frac{s}{(1+s)^K} \left[ \frac{1}{1 - (1+s)^{-K}} \right].\end{aligned}\quad (\text{B4})$$

In the competition-dominated regime,  $1/s$  sets the timescale of deme dynamics, see Eqs. (A3). The growth of the cluster of  $i$  mutant demes in time  $1/s$  is  $T^+(m, G, K)/s = mK E_G(i) \rho_M / (q_G s)$ . In the adopted coarse-grained description, slow migration is the regime where the invasion can be regarded as being instantaneous, with fixation of a successful  $M$  invader occurring before the next invasion. This requires that the average number of successful  $M$  invaders in the time for the on-deme dynamics is less than one,  $T^+(m, G, K)/s < 1$ , leading to the following condition for slow migration:

$$m < \frac{sq_G}{K\rho_M E_G(i)} < \frac{s}{K\rho_M}, \quad (\text{B5})$$

where we have used  $q_G/E_G(i) \leq 1$ . When  $s \ll 1$  and  $Ks \gg 1$ , we have  $\rho_M \sim s$  and therefore simply  $m < 1/K$ . For  $\Omega = 16, K = 100$  and  $s = 0.1$ , we can estimate that there is slow migration if  $m \lesssim 10^{-2}$ , which is in line with the values of  $m \in [10^{-5}, 10^{-2}]$  used in our examples, and matches where we see deviations in Fig. 2(d).

### Appendix C: Deme and metapopulation mean extinction times

In this section, we discuss the process of extinction of a single deme that has a constant carrying capacity  $K$  when  $\psi(m, K) \ll 1$ , see Sec. III 2. In this extinction-dominated regime, we can assume that the deme size rapidly fluctuates about  $K$ , and extinction occurs from a deme of constant size  $n(x) = K$  prior to any invasion. Without loss of generality (see below), we hence assume that extinction occurs from entirely occupied demes, with

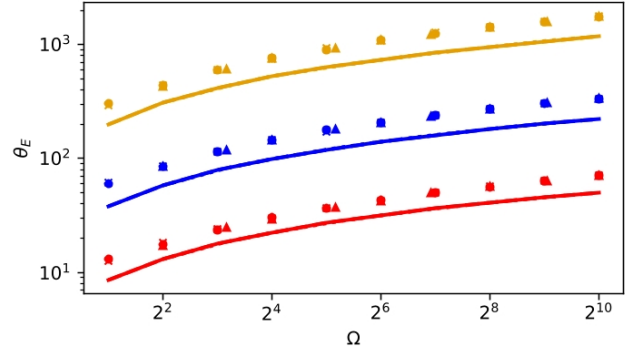


FIG. 8.  $\theta_E$  vs. metapopulation size  $\Omega$  for  $K = 7$  (yellow),  $K = 5$  (blue),  $K = 3$  (red) and  $m = 10^{-4}$ . Markers are simulation results and lines are predictions of Eq. (C4) for cliques (solid lines / crosses), cycles (dashed lines / circles), and grids (dotted lines / triangles). Markers of the same colour are almost indistinguishable. Deviations occur due to the approximation of  $\tau_E(K)$  in Eq. (C2). Selection plays no role in this regime, so results have been obtained with  $s = 0$ .

the metapopulation consisting only of  $W$  and  $M$  demes, all of size  $K$ . In this representation, the dynamics of a  $W/M$  deme when  $\psi \ll 1$  is given by the birth-death process of Sec. II with transition rates  $T_{W/M}^+ = n_{W/M}$  and  $T_{W/M}^- = n_{W/M}^2/K$ , subject to an absorbing boundary at  $n_{W/M} = 0$ , see Eq. (2). Clearly therefore, the deme dynamics is independent of its type, and the deme mean extinction time (dMET) is the average time to reach  $n_{W/M} = 0$  and is the same for  $W$  and  $M$  demes (dMET is independent of  $s$ ). A classical calculation yields (see, e.g. Sec. 6.7 in Ref. [71]) yields the following expression for an initially fully occupied deme of size  $K$ :

$$\tau_E(K) = \sum_{n=0}^{K-1} \left( \frac{n!}{K^n} \sum_{i=n+1}^{\infty} \frac{1}{i} \frac{K^i}{i!} \right). \quad (\text{C1})$$

The leading contribution to this expression arises from the term  $n=0$ :  $\tau_E(K) \simeq \sum_{i=1}^{\infty} K^i / (i \cdot i!)$ . This expression, corresponding to the dMET of a deme initialised with a single cell (of either type), is a good approximation of Eq. (C1) which indicates that the dMET is independent of selection and initial condition (for the leading order of  $\tau_E$ ). We can further simplify the leading contribution to the dMET by writing

$$\begin{aligned}\tau_E(K) &\simeq \sum_{n=1}^{\infty} \frac{K^n}{n!} \int_0^1 t^{n-1} dt, \\ &= \int_0^1 \frac{1}{t} \sum_{n=1}^{\infty} \frac{(Kt)^n}{n!} dt, \\ &= \int_0^K \frac{e^u - 1}{u} du,\end{aligned}$$

where we have used  $u = Kt$ . The main contribution to the last integral stem from the upper bound, yielding

$$\tau_E(K) \simeq \frac{e^K}{K}. \quad (\text{C2})$$

The dMET hence increases almost exponentially with  $K$ , is independent of the deme type, and its initial state.

The metapopulation mean extinction time (mMET) in the regime  $\psi(m, K) \ll 1$  can be obtained analytically within the realm of the above coarse-grained description, in the spirit of the approach of Ref. [59] for cliques. The metapopulation thus consists initially of entirely occupied demes ( $i$  mutant demes and  $\Omega - i$  type  $W$  demes). Since deme extinction here occurs prior to any invasion, we describe the metapopulation dynamics in terms of the number  $j = 0, 1, \dots, \Omega$  of entirely occupied demes. Residents (of either  $W$  or  $M$  type) of these filled demes can recolonise a neighbouring empty site at a rate  $B(j)$ , see Fig. 1(d). In addition, each occupied deme goes extinct at a rate  $D(j)$ . This coarse-grained description of the metapopulation dynamics is therefore a birth-death process with an absorbing state  $j = 0$  corresponding to the eventual extinction of the metapopulation, and a reflecting boundary at  $j = \Omega$  (all demes are occupied). In this picture, proceeding as above [71], the mMET reads

$$\theta_E(K, \Omega) = \sum_{n=1}^{\Omega-1} \left[ \left( \prod_{m=1}^{n-1} \frac{B(m)}{D(m)} \right) \sum_{j=n}^{\Omega} \frac{\prod_{l=1}^j \frac{B(l)}{D(l)}}{D(j)} \right]. \quad (\text{C3})$$

In the vein of Ref. [59] the recolonisation-birth rate of occupied demes is  $B(j) = mKj(1 - j/\Omega)$ , corresponding to a logistic growth with a rate proportional to the expected number of migrations from an occupied deme  $mK$ . Here, the extinction rate is  $D(j) = j/\tau_E$  and is inversely proportional to the mean local extinction time, that is the dMET. With  $\psi = mK\tau_E$ , using  $\prod_{l=n}^{j-1} (1 - \frac{l}{\Omega}) = \frac{1}{\Omega^{j-n}} \frac{(\Omega-n)!}{(\Omega-j)!}$ , Eq. (C3) can be rewritten as

$$\theta_E(K, \Omega) = \tau_E(K) \sum_{n=1}^{\Omega} \sum_{j=n}^{\Omega} \frac{1}{j} \left( \frac{\psi}{\Omega} \right)^{j-n} \frac{(\Omega-n)!}{(\Omega-j)!}. \quad (\text{C4})$$

In the extinction-dominated regime  $\psi \ll 1$ , the main contribution to the inner sum stems from  $j = n$ , and the leading contribution to the mMET is therefore

$$\theta_E(K, \Omega) \approx \tau_E(K) \sum_{n=1}^{\Omega} \frac{1}{n} = \tau_E(K) H_{\Omega}, \quad (\text{C5})$$

where  $H_{\Omega}$  is the  $\Omega$ -th harmonic number. Asymptotically, we have  $H_{\Omega} \simeq \ln(\Omega) + \gamma_{\text{EM}} + \mathcal{O}(\Omega^{-1})$  where  $\gamma_{\text{EM}} \approx 0.577\dots$  is the Euler-Mascheroni constant. This expression is independent of selection and, to leading order, generally does not depend on the initial state of the metapopulation. In the limit of a large metapopulation,  $\Omega \gg 1$ , the metapopulation mean extinction time in the

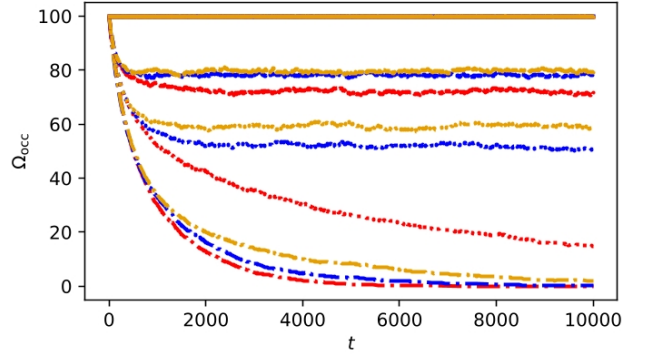


FIG. 9. *Metapopulation occupancy*:  $\Omega_{\text{occ}}$  vs.  $t$  for cliques (yellow), cycles (red), and grids (blue), with  $\Omega = 100$  and  $K = 8$ . Simulation results averaged on 100 realisations for the stationary number  $\Omega_{\text{occ}}$  of occupied demes for  $\psi = 100$  (solid lines),  $\psi = 5$  (dashed lines),  $\psi = 2.5$  (dotted lines), and  $\psi < 1$  (dash-dotted lines). Eq. (8) predicts  $\Omega_{\text{occ}} = 100, 80, 60, 0$  for  $\psi = 100, 5, 2.5$  and  $\psi < 1$ , respectively.

regime  $\psi(m, K) \ll 1$ , is asymptotically given by the simple expression Eq. (13):  $\theta_E(K, \Omega) \simeq \tau_E(\ln(\Omega) + \gamma_{\text{EM}})$ . When  $\Omega \gg 1$  and  $K \gg 1$ , we simply have  $\theta_E(K, \Omega) \simeq e^K \ln(\Omega)/K$ .

The result  $\theta_E(K, \Omega)$  has been explicitly derived for cliques (island model), but is found to provide good qualitative insight into the extinction dynamics for cycles and grids, see Fig. 2

#### Appendix D: Stationary deme occupancy

In the realm of the coarse-grained description of the extinction-dominated regime discussed in the previous section, we can use the rates  $B(j) = mKj(1 - j/\Omega)$  and  $D(j) = j/\tau_E$  to estimate the number of occupied demes  $\Omega_{\text{occ}}$  in the metapopulation when the environment is static (constant carrying capacity  $K$ ). At mean-field level, we can write the following balance equation [35]

$$\begin{aligned} \frac{d}{dt} \Omega_{\text{occ}} &= B(\Omega_{\text{occ}}) - D(\Omega_{\text{occ}}), \\ &= mK\Omega_{\text{occ}} \left( 1 - \frac{1}{\psi} - \frac{\Omega_{\text{occ}}}{\Omega} \right). \end{aligned} \quad (\text{D1})$$

The equilibria of this equation are  $\Omega_{\text{occ}} = 0$  and  $\Omega_{\text{occ}} = \Omega \frac{\psi-1}{\psi}$  when  $\psi > 1$ . The equilibrium  $\Omega_{\text{occ}} = 0$  is asymptotically stable when  $\psi < 1$  and unstable otherwise. This means that all demes go extinct, and there is extinction of the entire metapopulation when  $\psi < 1$ . When  $\psi > 1$ , the equilibrium  $\Omega_{\text{occ}} = \Omega \frac{\psi-1}{\psi}$  is asymptotically stable. This corresponds to a fraction  $1 - 1/\psi$  of the demes being entirely occupied, and there is fraction  $1/\psi$  of empty demes. In the limit where  $\psi \gg 1$ , we have  $\Omega_{\text{occ}} \rightarrow \Omega$  and all demes and hence the metapopulation are fully occupied. Putting everything together, we obtain Eq. (8).



This mean-field derivation of  $\Omega_{\text{occ}}$  is accurate for large clique metapopulations but, as it ignores spatial correlations, it is a crude approximation for cycles and grids, see Fig. 9. In particular,  $\Omega_{\text{occ}}$  overestimates the number of occupied demes in cycles when  $\psi$  is not much larger than 1. However,  $\psi = mK\tau_E$  allows us to distinguish between different regimes and provides a sound estimate of the number of occupied demes in the intermediate regime when  $\psi(m, K) \approx me^K$  is sufficiently bigger than 1.

### Appendix E: Average number of active edges on the square grid and the influence of the spatial structure

In principle, the coarse-grained description of the  $M/W$  competition holds for any regular circulation graph. However, this approach requires the determining of the number of active edges, which, except for cycles (one dimension) and cliques, is a difficult task due to complex spatial correlations between demes. Here, we consider the case of the square grid (with periodic boundaries), and illustrate how to estimate the average number of active edges when the metapopulation consists of only one single fully-occupied  $M$  deme and all other demes are occupied by  $W$  cells.

In the case of a large metapopulation,  $\Omega \gg 1$ , with unit spacing between neighbours, we assume that the mutant spreads outwards from the initial  $M$  deme approximately forming a  $M$ -cluster having a circular front. If this circular  $M$ -cluster has a radius  $r$ , it has an area  $\pi r^2$  containing a number  $i$  of  $M$  demes. The boundary of the circular  $M$ -cluster is of length  $2\pi r$ . Assuming that this length is equal to the number of  $M$  demes on the boundary, we find that  $r = \sqrt{i/\pi}$  and there are  $2\sqrt{i\pi}$  boundary demes given  $i$  demes of type  $M$ . We therefore estimate that the average number active edges for a grid is  $E_{\text{grid}}(i) \approx 2\sqrt{\pi i}$ . We have notably used this approximation in the transitions rates Eq. (10) and Eq. (19) for the coarse-grained description of  $M/W$  competition in static and time-varying environments in the regime of weak bottlenecks.

In Figs. 2(a,c) and 4(c), we have found that the spatial structure has a barely noticeable influence on the fixation probability and mean fixation time when the carrying capacity is constant and in time-varying environments in the regime of weak bottlenecks. Fig. 10 shows the heatmaps on a cycle and a grid metapopulation for the ‘‘idealised treatment’’ proposed in Sec. IV 2, which are almost identical. This is in accord with Eqs. (25) predicting that the same migration rate yields the same near optimal conditions for the heatmaps of metapopulation on any regular graph, here a cycle and a grid. Simulation results confirm spatial structure is only responsible for minor quantitative changes in the region of the heatmaps corresponding to the near-optimal ‘‘treatment conditions’’. This stems from the removal scenario characterising the idealised treatment being due to deme extinction which is mostly independent of  $G$  and  $m$ .

### Appendix F: Further details on the intermediate dynamics in static environments

In this section, we provide further details about the analysis of the intermediate dynamics in static environments, see Sec. III 3. Here, we complete the result given in the main text by considering metapopulation intermediate dynamics on a regular graph  $G$  ( $G$ -graph), obtaining the explicit results  $\phi_{\text{int}}^G$  and  $\theta_{\text{int}}^G$  for  $G = \{\text{clique, cycle, grid}\}$  reported in Fig. 11 when the metapopulation initially consists of a single  $M$  deme and  $\Omega - 1$  demes occupied by  $W$ .

The intermediate regime is characterised by  $M/W$  competition and deme extinction. Therefore, in addition to invasions, a  $W$  deme may become an  $M$  deme through extinction followed by a recolonisation, i.e.  $W \rightarrow \emptyset \rightarrow M$ , where  $\emptyset$  indicates an extinct deme. Similarly, an  $M$ -deme can be changed into a  $W$ -deme via  $M \rightarrow \emptyset \rightarrow W$ . We assume that there is initially a single  $M$  deme in the metapopulation (and  $\Omega - 1$  demes of type  $W$ ). With a probability  $p_{\text{surv}}$  (see below), the initial  $M$  deme survives to reach the dynamical equilibrium that consists of an unbreakable  $M$ -cluster whose size (number of  $M$  demes)  $i = 0, 1, \dots, \Omega_{\text{occ}}$  grows and shrinks through invasions and extinction-recolonisation events. We assume that immediately  $\Omega_E = \Omega/\psi$  demes go extinct, so that the metapopulation quickly reaches its equilibrium occupancy  $\Omega_{\text{occ}} = \Omega(1 - 1/\psi)$ . In this dynamical equilibrium, a  $W$  deme can become an  $M$  deme via  $W \rightarrow \emptyset$  ( $W$  deme extinction) at rate  $r_{\text{ext},W}$  followed by  $\emptyset \rightarrow M$  (recolonisation by  $M$ ) at rate  $r_{\text{rec},M}^G$ . The overall extinction-recolonisation reaction  $W \rightarrow \emptyset \rightarrow M$  thus occurs at rate  $1/(1/r_{\text{ext},W} + 1/r_{\text{rec},M}^G)$ . Here, the rate of  $W$  deme extinction is  $r_{\text{ext},W} = (\Omega_{\text{occ}} - i)/\tau_E$  and  $\tau_E$  is given by Eq. (6). We proceed similarly for the extinction of an  $M$  deme and its recolonisation into a  $W$  site according to  $M \rightarrow \emptyset \rightarrow W$ . Taking also into account the rate of invasion, see (10), the size  $i$  of the  $M$ -cluster on a  $G$ -regular graph varies according to the transition rates

$$\begin{aligned} \tilde{T}_i^+(m, G, K) &= mK \frac{E_G(i)}{q_G} \left[ \rho_M + \frac{1}{\psi - 1} \frac{q_G}{\Omega} \frac{i(\Omega_{\text{occ}} - i)}{E_G(i)} \right], \\ \tilde{T}_i^-(m, G, K) &= mK \frac{E_G(i)}{q_G} \left[ \rho_W + \frac{1}{\psi - 1} \frac{q_G}{\Omega} \frac{i(\Omega_{\text{occ}} - i)}{E_G(i)} \right]. \end{aligned} \quad (\text{F1})$$

With these rates, we can solve the following first-step analysis equations for the probability  $\phi_{\text{int},i}^G$  that the dynamical equilibrium comprising an initial  $M$ -cluster of size  $i$  contains only of occupied  $M$  demes after a mean time  $\theta_{\text{int},i}^G$ :

$$\begin{aligned} (\tilde{T}_i^+ + \tilde{T}_i^-) \phi_{\text{int},i}^G &= \tilde{T}_i^+ \phi_{\text{int},i+1}^G + \tilde{T}_i^- \phi_{\text{int},i-1}^G, \\ (\tilde{T}_i^+ + \tilde{T}_i^-) \theta_{\text{int},i}^G &= 1 + \tilde{T}_i^+ \theta_{\text{int},i+1}^G + \tilde{T}_i^- \theta_{\text{int},i-1}^G. \end{aligned} \quad (\text{F2})$$

These equations are subject to the boundary conditions  $\phi_{\text{int},0}^G = 0, \phi_{\text{int},\Omega_{\text{occ}}}^G = 1$  and  $\theta_{\text{int},0}^G = \theta_{\text{int},\Omega_{\text{occ}}}^G = 0$ . We thus have  $\phi_{\text{int}}^G \equiv p_{\text{surv}} \phi_{\text{int},1}^G$  and  $\theta_{\text{int}}^G \equiv p_{\text{surv}} \theta_{\text{int},1}^G + (1 -$

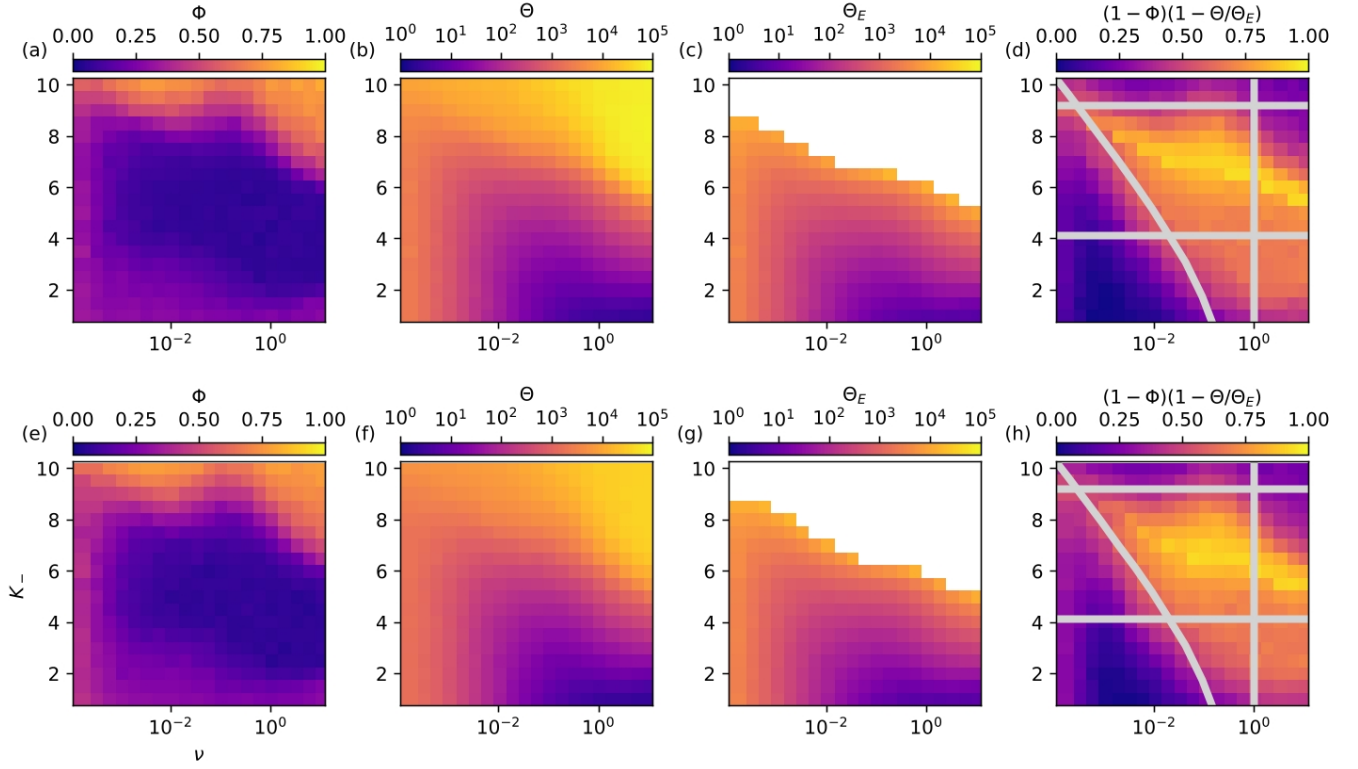


FIG. 10. Near-optimal condition for the idealised treatment on a cycle and grid metapopulation.  $(\nu, K_-)$  heatmaps of  $\Phi$ ,  $\Theta$ ,  $\Theta_E$  and  $(1 - \Phi)(1 - \Theta/\Theta_E)$  for the cycle (a-d) and grid (e-h) metapopulations, see Appendix E. Whitespace in panels (c) and (g) indicate the region of the parameter where at least one realisation for those parameters did not reach extinction by  $t = 10^5$ . Grey lines in panels (d) and (h) show the near-optimal conditions for the idealised treatment:  $\psi(m, K_-) < 1$  below the top horizontal line,  $mK_+\theta_E > 1$  above the bottom horizontal line, and  $\nu\theta_E > 1$  above the curved line, while the vertical line indicates where  $\nu < 1$  and  $\theta_E$  from Eq. (13). The near-optimal treatment conditions is the yellowish cloud at the centre of the area enclosed by these lines. Other parameters are  $\Omega = 16$ ,  $m = 10^{-4}$ ,  $s = 0.1$ , and  $K_+ = 200$ . In all panels, initially there is a single  $M$  deme and  $\Omega - 1$  demes occupied by  $W$ .

$p_{\text{surv}}\tau_E$ . The factor  $p_{\text{surv}} = \frac{\Gamma(\Omega)}{\Gamma(\Omega_{\text{occ}})} \frac{1}{\Omega^{\Omega_{\text{occ}}}}$  is the probability that the initial  $M$  deme reaches the dynamical equilibrium, while the contribution  $(1 - p_{\text{surv}})\tau_E$  to  $\theta_{\text{int}}^G$  accounts for the probability that the initial  $M$  deme goes extinct in a mean time  $\tau_E$  (given by Eq. (6)) before reaching the equilibrium. The final expressions of  $\phi_{\text{int}}^G$  and  $\theta_{\text{int}}^G$  thus read

$$\begin{aligned} \phi_{\text{int}}^G &= p_{\text{surv}} \frac{1}{1 + \sum_{k=1}^{\Omega_{\text{occ}}-1} \prod_{m=1}^k \tilde{\gamma}(m)}, \\ \theta_{\text{int}}^G &= \phi_{\text{int}}^G \sum_{k=1}^{\Omega_{\text{occ}}-1} \sum_{n=1}^k \frac{\prod_{m=n+1}^k \tilde{\gamma}(m)}{\tilde{T}_n^+} + (1 - p_{\text{surv}})\tau_E, \end{aligned} \quad (\text{F3})$$

where

$$\tilde{\gamma}_G(i) \equiv \frac{\rho_W + \frac{1}{\psi-1} \frac{q_G}{\Omega} \frac{i(\Omega_{\text{occ}}-i)}{E_G(i)}}{\rho_M + \frac{1}{\psi-1} \frac{q_G}{\Omega} \frac{i(\Omega_{\text{occ}}-i)}{E_G(i)}}, \quad (\text{F4})$$

and the upper limit of the first sum in  $\phi_{\text{int}}^G$  and  $\theta_{\text{int}}^G$  is rounded to the nearest integer. We find that  $\phi_{\text{int}}^G$  depends on the migration rate  $m$ , carrying capacity  $K$ , and

the spatial structure  $G$  via  $\tilde{\gamma}_G$  and  $\Omega_{\text{occ}}$ . In the case of the clique discussed in the main text, the expression of Eq. (F4) simplifies to

$$\tilde{\gamma}_{\text{clique}}(i) \equiv \tilde{\gamma}_{\text{clique}} = \frac{\rho_W + \frac{1}{\psi-1}}{\rho_M + \frac{1}{\psi-1}}. \quad (\text{F5})$$

We notice that for all graphs  $G$ , the expressions of Eq. (F3) coincide with those of Eq. (12) of the competition-dominated regime, with  $\tilde{\gamma}_G(i) \xrightarrow{\psi \gg 1} \gamma = \rho_W/\rho_M$ . In Fig. 11, we find that the predictions of Eq. (F3) are in good agreement with simulation results for all spatial structures  $G$ . Moreover, we notice that the spatial dependence of  $\phi_{\text{int}}^G$  and  $\theta_{\text{int}}^G$  is barely noticeably.

### Appendix G: Fixation probability in time-switching environments under weak bottlenecks

In this section, we discuss in further detail the dependence of the fixation probability  $\Phi^G(\nu, m)$  on the migra-

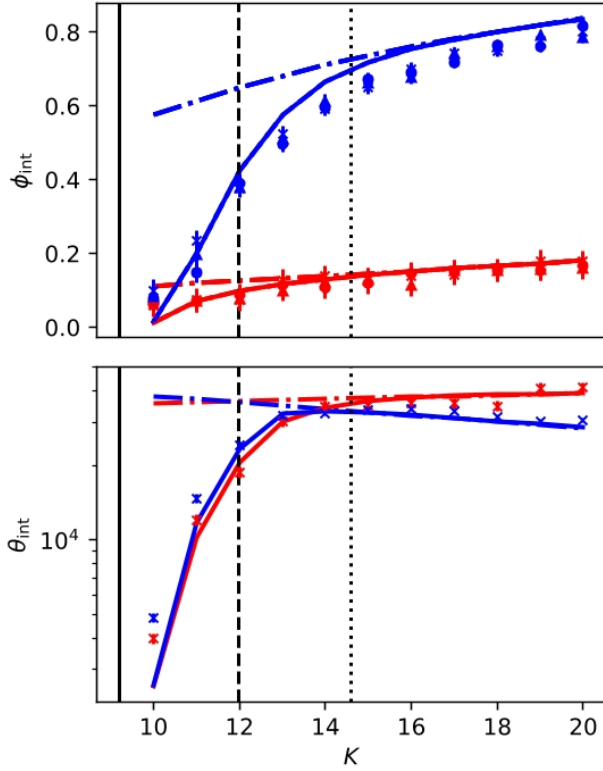


FIG. 11.  $\phi_{\text{int}}$  vs.  $K$  for  $s = 0.1$  (blue) and  $s = 0.01$  (red) on clique (solid lines / crosses), cycle (dashed lines / circles), and a grid (dotted lines / triangles). The different symbols and lines are almost indistinguishable.  $\theta_{\text{int}}$  vs.  $K$  for the same parameters for a clique metapopulation. The vertical solid and dashed line indicate where the number of occupied demes  $\Omega_{\text{occ}} \in [1, \Omega - 1]$ , see text. The dotted line indicates where  $\psi = \Omega K$ , i.e. every individual migrates in the time required for an independent deme extinction. Markers show simulation results, solid lines are predictions of Eq. (F3), and dash-dot lines are predictions of Eq. (12). Other parameters are  $m = 10^{-4}$  and  $\Omega = 16$ .

tion rate  $m$  and spatial structure  $G$  of the metapopulation in time-switching environments under weak bottlenecks.

In static environments, where  $K$  is constant, a generalisation of the circulation theorem guarantees that the fixation probability is independent on the migration rate and spatial structure of the metapopulation arranged on a circulation graph, see Eq. (12). This results from a correspondence between the fixation probability and the number of  $M$  demes performing a biased random walk on  $[0, \Omega]$  with a bias that is independent of  $m$  and  $G$  [41].

In time-switching environments under weak bottlenecks (deme extinction is negligible) the correspondence is between the fixation  $\Phi^G(\nu, m)$  and the random walk (with absorbing boundaries) on  $[0, \Omega] \times \{-1, 1\}$  for the number of fully mutant demes in the environmental state  $\xi = \pm 1$ . As a consequence,  $\Phi^G(\nu, m)$  is the probability of absorption in the state  $\Omega$ . In this setting, defining the

state of the random walk by  $(i, \xi)$ , where  $i = 0, 1, \dots, \Omega$ , the random walk moves to the right ( $i \rightarrow i + 1$ ) with a probability  $r(i, \xi)$ , to the left ( $i \rightarrow i - 1$ ) with a probability  $\ell(i, \xi)$ , or switches environment ( $\xi \rightarrow -\xi$ ) with probability  $\epsilon(i, \xi)$ , where

$$\begin{aligned} r(i, \xi) &= \frac{m\mathcal{N}_\xi(\nu) \frac{E_G(i)}{q_G} \rho_{M,\xi}(\nu)}{m\mathcal{N}_\xi(\nu) \frac{E_G(i)}{q_G} \rho_{M,\xi}(\nu) + m\mathcal{N}_\xi(\nu) \frac{E_G(i)}{q_G} \rho_{W,\xi}(\nu) + \nu}, \\ \ell(i, \xi) &= \frac{m\mathcal{N}_\xi(\nu) \frac{E_G(i)}{q_G} \rho_{W,\xi}(\nu)}{m\mathcal{N}_\xi(\nu) \frac{E_G(i)}{q_G} \rho_{M,\xi}(\nu) + m\mathcal{N}_\xi(\nu) \frac{E_G(i)}{q_G} \rho_{W,\xi}(\nu) + \nu}, \\ \epsilon(i, \xi) &= \frac{\nu}{m\mathcal{N}_\xi(\nu) \frac{E_G(i)}{q_G} \rho_{M,\xi}(\nu) + m\mathcal{N}_\xi(\nu) \frac{E_G(i)}{q_G} \rho_{W,\xi}(\nu) + \nu}. \end{aligned} \quad (\text{G1})$$

$\Phi^G(\nu, m)$  thus coincides with the probability that the random walk defined by Eq. (G1) gets absorbed in the state  $i = \Omega$ . For the fixation probability to be independent of  $m$  and  $G$  then requires each of  $r(i, \xi)$ ,  $\ell(i, \xi)$ , and  $\epsilon(i, \xi)$  to be independent of  $m$  and  $G$ . However, this is generally not the case in the presence of environmental switching ( $\nu > 0$ ) due to the explicit and implicit dependence of Eq. (G1) on  $\nu$  (in the denominator and via  $\mathcal{N}$  and  $\rho_{M/W}$ ). This implies that in time-fluctuating environments the fixation probability  $\Phi^G(\nu, m)$  is expected to depend on  $m$  and  $G$ .

Interestingly however, Fig. 4(c) illustrates the almost unnoticeable dependence of  $\Phi^G(\nu, m)$  on the specific spatial structure. This is due to the overall similar impact of the factor  $E_G(i)/q_G$  for the various graphs. While differences arise when  $m$  varies at fixed  $\nu$  due to large variations in the timescales of the competition dynamics (significantly more invasions when  $K = K_+$  than when  $K = K_-$ ), varying spatial structure produces small changes in these timescales, and as such leads to only unnoticeable changes in  $\Phi$ .

#### Appendix H: Asymmetric dichotomous Markov noise & environmental bias

For the sake of simplicity and clarity, in the main text we have focused on symmetric environmental switching. In this section, we relax this assumption and outline how the results of the paper can be generalised to the case when there is an environmental bias, i.e. when there is a different average time spent in the states  $\xi = \pm 1$ .

Here, we consider the coloured asymmetric dichotomous Markov noise (aDMN), also called telegraph process,  $\xi(t) \in \{-1, 1\}$  that switches between  $\pm 1$  according to  $\xi \rightarrow -\xi$  at rate  $\nu_\pm$  when  $\xi = \pm 1$  [68–70]. It is convenient to write these asymmetric switching rates as  $\nu_\pm = \nu(1 \mp \delta)$ , where  $\nu \equiv (\nu_- + \nu_+)/2$  is the mean switching rate,  $\delta \equiv (\nu_- - \nu_+)/(\nu_- + \nu_+) = (\nu_- - \nu_+)/2\nu$  denotes the switching bias, with  $|\delta| \leq 1$  and  $\delta > 0$  when more time is spent on average in the mild environment [18, 19]. At stationarity, this aDMN has average

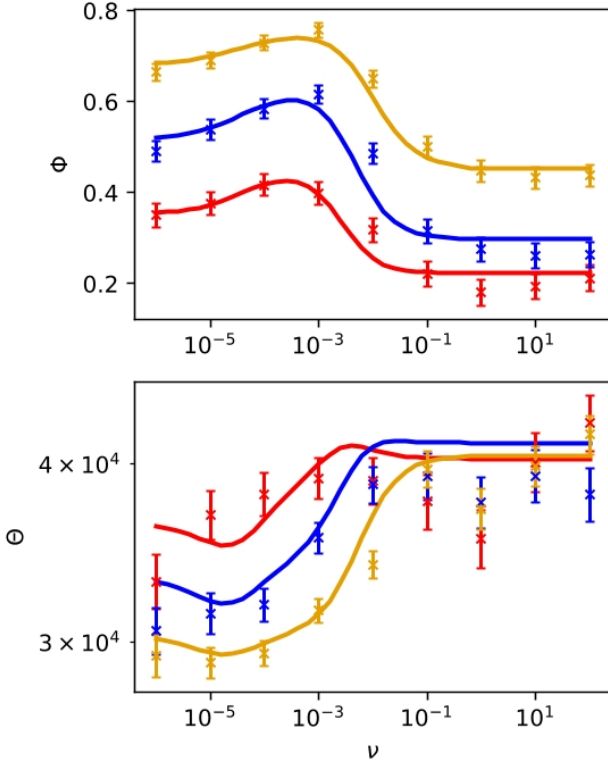


FIG. 12. Fixation probability  $\Phi^G$  and mean fixation time  $\Theta^G$  against switching rate  $\nu$  for different values of  $\delta$ . Red, blue, and yellow represent  $\delta = -0.5$ ,  $\delta = 0.0$ , and  $\delta = 0.5$ , respectively. Markers show simulation results and lines are predictions of Eq. (24). Other parameters are  $\Omega = 16$ ,  $s = 0.01$ ,  $m = 10^{-4}$ ,  $K_+ = 200$ , and  $K_- = 20$ .

$\langle \xi(t) \rangle = \delta$  and autocovariance  $\langle \xi(t)\xi(t') \rangle - \langle \xi(t) \rangle \langle \xi(t') \rangle = (1 - \delta^2)e^{-2\nu|t-t'|}$  [16, 17, 68–70].

The aDMN drives the *time-switching* carrying capacity

$$K(t) = \frac{1}{2} [K_+ + K_- + \xi(t)(K_+ - K_-)], \quad (\text{H1})$$

which is the same expression as Eq. (5), but now driven by the aDMN  $\xi(t)$  [16–19, 21, 22, 32]. The carrying capacity switches back and forth from  $K_+$  (mild environment,  $\xi = 1$ ) to  $K_- < K_+$  (harsh environment,  $\xi = -1$ ) at rate  $\nu_{\pm} = \nu(1 \mp \delta)$  according to

$$K_+ \xrightleftharpoons[\nu_- = \nu(1+\delta)]{\nu_+ = \nu(1-\delta)} K_-.$$

At stationarity, the expected value of the carrying capacity is  $\langle K(t) \rangle = \frac{1}{2}(K_+ + K_- + \delta(K_+ - K_-))$ , and its auto-covariance is  $\langle K(t)K(t') \rangle - \langle K(t) \rangle \langle K(t') \rangle = \left(\frac{K_+ - K_-}{2}\right)^2 (1 - \delta^2) e^{-2\nu|t-t'|}$  [68–70].

Under asymmetric switching, the stationary population distribution of a single deme, both in the absence and presence of migration (see Appendix A 2), is well approximated by stationary density of the piecewise Markov

process Eq. (A4) ( $n$ -PDMP), now driven by the aDMN, whose joint density is

$$p_{\xi}(\nu, \delta, n) \propto \begin{cases} \frac{1+\delta}{n^2} \left(\frac{K_+ - n}{n}\right)^{\nu(1-\delta)-1} \left(\frac{n - K_-}{n}\right)^{\nu(1+\delta)} & \text{if } \xi = 1, \\ \frac{1-\delta}{n^2} \left(\frac{K_+ - n}{n}\right)^{\nu(1-\delta)} \left(\frac{n - K_-}{n}\right)^{\nu(1+\delta)-1} & \text{if } \xi = -1, \end{cases} \quad (\text{H2})$$

where the proportional factor accounts for the normalisation constants. The stationary marginal density of this  $n$ -PDMP, up to the normalisation constant, is

$$p(\nu, \delta, n) = \sum_{\xi} \left(\frac{1 + \xi\delta}{2}\right) p_{\xi}(\nu, \delta, n), \\ \propto \frac{1}{n^2} \left(\frac{K_+ - n}{n}\right)^{\nu(1-\delta)-1} \left(\frac{n - K_-}{n}\right)^{\nu(1+\delta)-1}, \quad (\text{H3})$$

where we have again omitted the normalisation constant. The  $n$ -PDMP density captures the mean features of the deme size distribution: It is bimodal with peaks at  $K_+$  and  $K_-$  ( $n \approx K_{\pm}$ ) when  $\nu \ll 1$ , and is unimodal and centred around  $n \approx 2K_+K_- / [(1 - \delta)K_+ + (1 + \delta)K_-]$  when  $\nu \gg 1$  [18, 21, 22, 24, 32]. When  $\nu(1 \pm \delta) \lesssim 1$ , the size  $n$  of each deme tracks the carrying capacity, and a bottleneck occurs at an average frequency  $\nu_+ \nu_- / (2\nu) = \nu(1 - \delta^2)/2$ , each time  $K$  switches from  $K_+$  to  $K_-$  [18, 21, 32].

In the realm of the coarse-grained description discussed in the main text, the regime of weak bottlenecks dominated by the  $W/M$  competition can be characterised by the  $M$  fixation probability  $\Phi^G(\nu, \delta, m)$  and unconditional mean fixation time  $\Theta^G(\nu, \delta, m)$  by Eq. (24) obtained by solving the first-step analysis equations Eq. (21) and Eq. (22) with the transition rates Eq. (19) and Eq. (20) obtained using  $N_{\xi}(\nu, \delta)$  averaged over Eq. (H3), i.e.  $N_{\xi}(\nu, \delta) = \int n p_{\xi}(\nu, \delta, n) dn$ . The results of Fig. 12 for a cycle metapopulation show that the predictions coarse-grained description based on the PDMP approximation Eq. (H3) are in good agreement with simulation results.  $\Phi^G(\nu, \delta, m)$  and  $\Theta^G(\nu, \delta, m)$  are again found to exhibit a non-monotonic dependence on  $\nu$ , with extrema in the range of intermediate  $\nu$ . The main effect of  $\delta$  is to increase the  $M$  fixation probability and reduce the mean fixation time when  $\delta > 0$ , which is intuitively clear since this corresponds to a bias towards the mild state favouring the fixation of  $M$ .

The regime of strong bottlenecks is dominated by the interplay between  $M/W$  competition in the mild state ( $K = K_+$ ) and deme extinction in the harsh environmental state ( $K = K_-$ ), occurring in time  $\theta_E \equiv \theta_E(K_-, \Omega)$ . In this regime, the near-optimal conditions for the removal of the mutant strain can be obtained as under symmetric switching (given by Eq. (25)) and now read:

$$\psi(m, K_-) < 1, \quad \nu(1 \pm \delta) \lesssim 1, \\ \nu(1 + \delta)\theta_E \gtrsim 1, \quad mK_+\theta_E \frac{1 + \delta}{1 - \delta} \gtrsim 1, \quad (\text{H4})$$

which, as Eq. (25), are conditions depending on  $m$  but

not on the spatial structure  $G$ . The main differences from Eq. (25) are in the conditions  $\theta_E \nu_- = \theta_E \nu (1 + \delta) \gtrsim 1$  and  $mK_+ \theta_E \frac{\nu_-}{\nu_+} = mK_+ \theta_E \frac{1+\delta}{1-\delta} \gtrsim 1$ . The first of these changes ensures that a switch occurs before the metapopulation mean extinction time in the harsh environment,  $\theta_E$ . The second ensures there are enough recolonisations in the mild environment to maintain the metapopulation given the minimum switching rate required to prevent extinction in the harsh environment, i.e. rearranging  $\theta_E \nu_- \gtrsim 1$  gives  $\nu \gtrsim 1/(\theta_E(1 + \delta))$  and for sufficient recolonisations we require  $mK_+/\nu_+ \equiv mK_+/(\nu(1 - \delta)) \gtrsim 1$ , where we substitute our expression for  $\nu$ . Since  $\theta_E$  is independent of  $\delta$ , we expect that the conditions Eq. (H4) define a region in the parameter space that is similar to that obtained under symmetric switching, shifted towards higher (lower) values of  $\nu$  and  $K_-$  when  $\delta < 0$  ( $\delta > 0$ ). This picture is confirmed by the heatmaps of Fig. 13.

### Appendix I: Simulation methods & plots

In this section, we explain how the simulation of the individual-based dynamics of the full model have been implemented. We also outline how we have plotted the simulation/numerical data that we have obtained to produce the figures discussed in the main text and appendices.

In addition to the coarse-grained descriptions of the model that provide us with analytical approximations of metapopulation dynamics in different regimes, we have employed Monte Carlo (MC) methods to simulate the full individual-based model and mirror the dynamics encoded in the ME Eq. (A2). In this section, we outline how we have performed the stochastic simulations that we have notably used to test our analytical predictions.

While not exact like other simulation methods (e.g. the Gillespie algorithm [98]), the Monte Carlo algorithm used here improves on computational efficiency making simulations with larger numbers of cells on the metapopulation that run for long times feasible. The questions of computational efficiency and tractability are particularly critical in the context of this work in which we study fixation and extinction of spatially arranged populations, a notoriously computationally demanding problem.

In the case of symmetric environmental switching, the MC algorithm that we have employed can be described as follows: The graph, consisting of the spatially arranged  $\Omega$  deme forming the metapopulation, is initialised by randomly picking an initial value for the carrying capacity  $K(0) = \{K_-, K_+\}$  with equal probability (in the constant environment case  $K(0) = K$  with probability 1), populating a single deme with  $K(0)$   $M$ -cells, and the remaining  $\Omega - 1$  of the demes with  $K(0)$   $W$ -cells. Time is then discretised in units of Monte Carlo steps (MCS) whereby in each MCS we perform  $2N$  birth and death events, where  $N$  is measured at the start of the MCS. We choose  $2N$  as we typically have  $N$  births and  $N$  deaths per unit time according to the transition rates Eq. (2) and

Eq. (4) when summing over all cells on the metapopulation. Therefore, our units of time are consistent between the theoretical model and the Monte Carlo simulation. Each of the  $2N$  events in an MCS occur sequentially and the rates are updated for the next event in the MCS. The type of each of the  $2N$  events within an MCS is selected based on the rates of the events, where a higher rate means a larger probability of that event being selected. Concretely, the following steps for a single MCS occur:

- Check if an environmental switch, occurring with rate  $\nu$ , occurs on the metapopulation. The rate of reaction of birth/death/migration events on the entire metapopulation is  $N(1 + m + N/K(t))$ . Therefore, the probability of an environmental switch is given by  $\nu/(N(1 + m + N/K(t) + \nu))$ .
- Otherwise, a deme  $x$  is picked for an event to occur based on the total rate of events on that deme,  $n(x)(1 + m + n(x)/K(t))$ . Therefore, the probability of selecting a deme  $x$  for an event is  $\frac{n(x)(1+m+n(x)/K(t))}{N(1+m+N/K(t))}$ .
- A species is picked for an event to occur based on the total rate of events of that species on the selected deme. The propensity of a given species  $\alpha$  on deme  $x$  is  $n_\alpha(x)(1 + m + n(x)/K(t))$ , and the total rate of events on the deme is as in the previous step. Therefore, that species is selected with probability  $\frac{n_\alpha(x)(1+m+n(x)/K(t))}{n(x)(1+m+n(x)/K(t))} = \frac{n_\alpha(x)}{n(x)}$ .
- The species on the deme can then either undergo a birth, death, or migration event, with the probability of each depending on the rates of these events. Birth, death, or migration is selected with probability  $\frac{T_\alpha^{+, -, m}(x)}{n_\alpha(x)(1+m+n(x)/K(t))}$ .
- The selected event is performed.
- The above steps are repeated until  $2N$  births and deaths events are performed.

In all simulations, each realisation is simulated until fixation, tracking when fixation occurs and which species fixates. In simulations for Figs. 2(e-g), 6, 10, and 13 the simulation then continues until metapopulation extinction or a large fixed time  $T$  (here we set  $T = 10^5$ ). For a given set of parameters, if extinction does not occur in any realisation, the extinction time is not recorded. The data is averaged to obtain the fixation probability, the mean fixation time, and the mean time to extinction where applicable. Furthermore, we record the standard error on the mean for each quantity. In Figs. 2, 4, and 12,  $10^3$  realisations are ran for each set of parameters, and these data are plotted with the standard error on the mean shows as error bars. In the heatmaps, each data point corresponds to the average value for  $10^3$  simulations at that point in parameter space. The standard error on the mean is not plotted for the heatmaps.

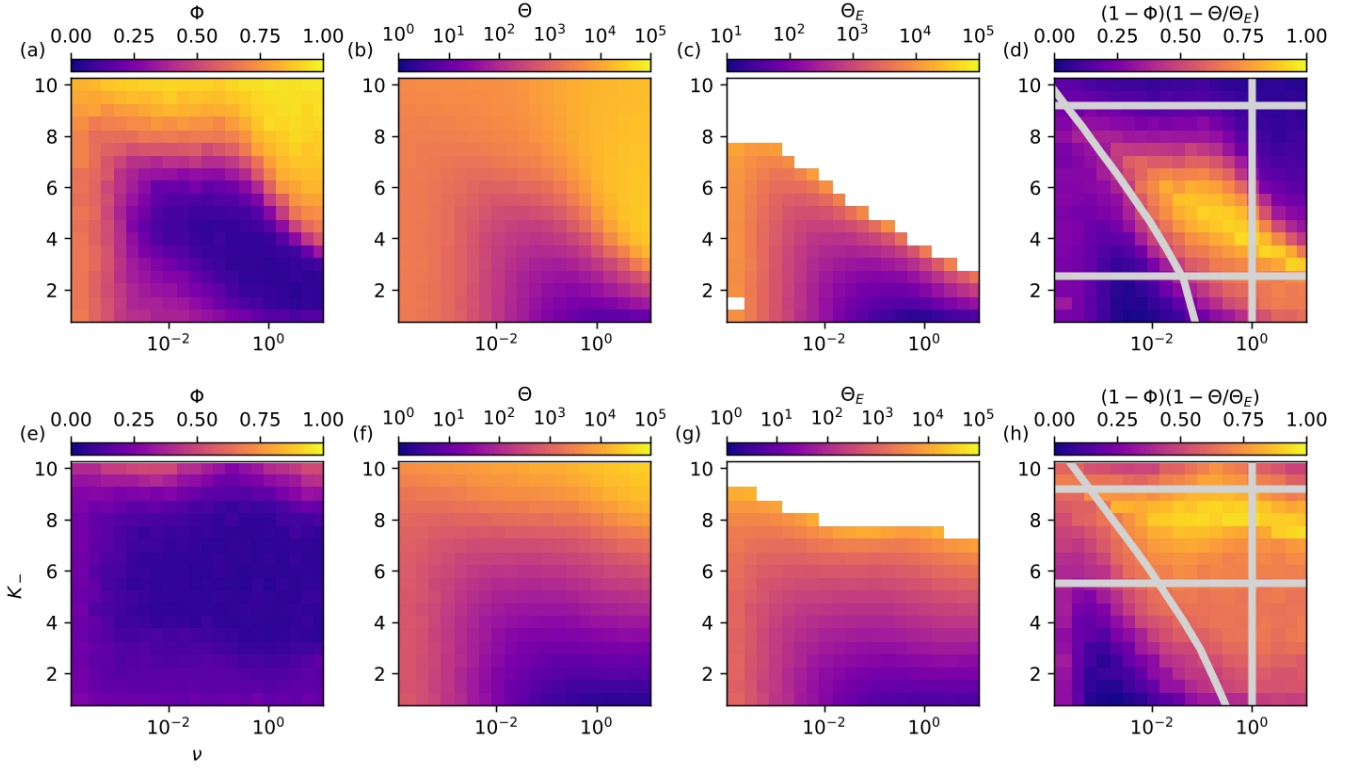


FIG. 13. Near-optimal condition for the idealised treatment on the clique metapopulation.  $(\nu, K_-)$  heatmaps of  $\Phi$ ,  $\Theta$ ,  $\Theta_E$  and  $(1 - \Phi)(1 - \Theta/\Theta_E)$  for the  $\delta = 0.5$  (a-d) and  $\delta = -0.5$  (e-h) metapopulations, see Appendix H. Whitespace in panels (c) and (g) indicate the region of the parameter where at least one realisation for those parameters did not reach extinction by  $t = 10^5$ . Grey lines in panels (d) and (h) show the near-optimal conditions for the idealised treatment in the asymmetric environment:  $\psi(m, K_-) < 1$  below the top horizontal line,  $mK_+ \theta_E \frac{1+\delta}{1-\delta} > 1$  above the bottom horizontal line, and  $\nu(1 + \delta)\theta_E > 1$  above the curved line, while the vertical line indicates where  $\nu < 1$  and  $\theta_E$  from Eq. (13). The near-optimal treatment conditions is the yellowish cloud at the centre of the area enclosed by these lines. Other parameters are  $\Omega = 16$ ,  $m = 10^{-4}$ ,  $s = 0.1$ , and  $K_+ = 200$ . In all panels, initially there is a single  $M$  deme and  $\Omega - 1$  demes occupied by  $W$ .

In the case that  $K(t) = K = \text{constant}$ , we set  $\nu = 0$  and  $K_+ = K_- = K$ , such that the first step of the above process is effectively skipped. In the case that the switching is asymmetric, the starting state is chosen according to the stationary distribution of  $K(t)$ , i.e.  $K(0) = K_{\pm}$

with probability  $\frac{1 \pm \delta}{2}$ . The probability for an environmental switch in the first step then depends on the current environmental state, where a switch occurs with probability  $\nu_{\pm}/(N(1 + m + N/K(t)) + \nu_{\pm})$  for  $K(t) = K_{\pm}$ .

- 
- [1] S. Widder and *et al.*, Challenges in microbial ecology: building predictive understanding of community function and dynamics, *ISME J.* **10**, 2557 (2016).
- [2] P. Engel and N. Moran, The gut microbiota of insects—diversity in structure and function, *FEMS Microbiol Rev.* **37**, 699 (2013).
- [3] N. Garud, B. Good, O. Hallatschek, and K. Pollard, Evolutionary dynamics of bacteria in the gut microbiome within and across hosts, *PLoS Biol* **17**, e3000102 (2019).
- [4] J. J. She and *et al.*, Defining the biogeographical map and potential bacterial translocation of microbiome in human surface organs, *Nature Communications* **15**, 427 (2024).
- [5] F. Cignarella and *et al.*, Intermittent fasting confers protection in cns autoimmunity by altering the gut microbiota, *Cell Metab.* **27**, 1222 (2018).
- [6] S. A. Smits and *et al.*, Seasonal cycling in the gut microbiome of the hadza hunter-gatherers of tanzania, *Science* **357**, 802 (2017).
- [7] W. Ewens, *Mathematical Population Genetics* (Springer, New York, 2004).
- [8] J. F. Crow and M. Kimura, *An Introduction to Population Genetics Theory* (Blackburn Press, Caldwell, NJ, USA, 2009).
- [9] J. Roughgarden, *Theory of Population Genetics and Evolutionary Ecology: An Introduction* (Macmillan, New York, USA, 1979).
- [10] A. Melbinger, J. Cremer, and E. Frey, Evolutionary game theory in growing populations, *Phys. Rev. Lett.* **105**,



- 178101 (2010).
- [11] J. Cremer, A. Melbinger, and E. Frey, Frey, evolutionary and population dynamics: A coupled approach, *Phys. Rev. E* **84**, 051921 (2011).
- [12] J. Cremer, A. Melbinger, and E. Frey, Growth dynamics and the evolution of cooperation in microbial populations, *Scientific Reports* **2**, 281 (2012).
- [13] A. Melbinger, J. Cremer, and E. Frey, The emergence of cooperation from a single mutant during microbial life cycles, *J. R. Soc. Interface* **12**, 20150171 (2015).
- [14] J. S. Chuang, O. Rivoire, and S. Leibler, Simpson's paradox in a synthetic microbial system, *Science* **323**, 20150171 (2009).
- [15] N. Verdon, O. Popescu, S. Titmuss, and R. J. Allen, Habitat fragmentation enhances microbial collective defence, *J. R. Soc. Interface* **22**, 20240611 (2025).
- [16] K. Wienand, E. Frey, and M. Mobilia, Evolution of a Fluctuating Population in a Randomly Switching Environment, *Phys. Rev. Lett.* **119**, 158301 (2017).
- [17] K. Wienand, E. Frey, and M. Mobilia, Eco-evolutionary dynamics of a population with randomly switching carrying capacity, *J. R. Soc. Interface* **15**, 20180343 (2018).
- [18] A. Taitelbaum, R. West, M. Assaf, and M. Mobilia, Population Dynamics in a Changing Environment: Random versus Periodic Switching, *Physical Review Letters* **125**, 048105 (2020).
- [19] A. Taitelbaum, R. West, M. Mobilia, and M. Assaf, Evolutionary dynamics in a varying environment: Continuous versus discrete noise, *Physical Review Research* **5**, L022004 (2023).
- [20] S. Shibusaki, M. Mobilia, and S. Mitri, Exclusion of the fittest predicts microbial community diversity in fluctuating environments, *Journal of The Royal Society Interface* **18**, 20210613 (2021).
- [21] L. Hernández-Navarro, M. Asker, A. M. Rucklidge, and M. Mobilia, Coupled environmental and demographic fluctuations shape the evolution of cooperative antimicrobial resistance, *Journal of The Royal Society Interface* **20**, 20230393 (2023).
- [22] M. Asker, L. Hernández-Navarro, A. M. Rucklidge, and M. Mobilia, Coexistence of Competing Microbial Strains under Twofold Environmental Variability and Demographic Fluctuations, *New Journal of Physics* **25**, 123010 (2023).
- [23] R. West and M. Mobilia, Fixation properties of rock-paper-scissors games in fluctuating populations, *J. Theor. Biol.* **491**, 110135 (2020).
- [24] L. Hernández-Navarro, M. Asker, and M. Mobilia, Eco-evolutionary dynamics of cooperative antimicrobial resistance in a population of fluctuating volume and size, *Journal of Physics A: Mathematical and Theoretical* **57**, 265003 (2024).
- [25] L. M. Wahl, P. J. Gerrish, , and I. Saika-Voivod, Evaluating the impact of population bottlenecks in experimental evolution, *Genetics* **162**, 961 (2002).
- [26] P. B. Rainey and K. Rainey, Evolution of cooperation and conflict in experimental bacterial populations, *Nature (London)* **425**, 72 (2003).
- [27] Z. Patwa and L. M. Wahl, Adaptation Rates of Lytic Viruses Depend Critically on Whether Host Cells Survive the Bottleneck, *Evolution* **64**, 1166 (2010).
- [28] M. A. Brockhurst, A. Buckling, and A. Gardner, Cooperation peaks at intermediate disturbance, *Curr. Biol.* **17**, 761 (2007).
- [29] M. A. Brockhurst, Population bottlenecks promote cooperation in bacterial biofilms, *PLoS One* **2**, e634 (2007).
- [30] J. Coates, B. R. Park, D. Le, E. Şimşek, W. Chaudhry, and M. Kim, Antibiotic-induced population fluctuations and stochastic clearance of bacteria, *eLife* **7**, e32976 (2018).
- [31] N. Mahrt, A. Tietze, S. Künzel, S. Franzenburg, C. Barbosa, G. Jansen, and H. Schulenburg, Bottleneck size and selection level reproducibly impact evolution of antibiotic resistance, *Nature Ecology & Evolution* **5**, 1233 (2021).
- [32] L. Hernández-Navarro, K. Distefano, U. C. Täuber, and M. M, Slow spatial migration can help eradicate cooperative antimicrobial resistance in time-varying environments (2024), [bioRxiv:2024.12.30.630406](https://arxiv.org/abs/2024.12.30.630406).
- [33] S. Wright, Evolution in Mendelian Populations, *Genetics* **16**, 97 (1931).
- [34] M. Kimura and G. H. Weiss, The Stepping Stone Model of Population Structure and the Decrease of Genetic Correlation with Distance, *Genetics* **49**, 561 (1964).
- [35] R. Levins, Some demographic and genetic consequences of environmental heterogeneity for biological control, *Bull. Entomol. Soc. Am.* **15**, 237 (1969).
- [36] I. Hanski, *Metapopulation Ecology* (Oxford University Press, New York, USA, 1999).
- [37] C. Lugo and A. J. McKane, Quasicycles in a spatial predator-prey model, *Phys. Rev. E* **78**, 051911 (2008).
- [38] T. Butler and N. Goldenfeld, Robust ecological pattern formation induced by demographic noise, *Phys. Rev. E* **80**, 030902(R) (2009).
- [39] B. Szczesny, M. Mobilia, and A. M. Rucklidge, Characterization of spiraling patterns in spatial rock-paper-scissors games, *Phys. Rev. E* **90**, 032704 (2014).
- [40] F. Peruzzo, M. Mobilia, and S. Azaele, Spatial patterns emerging from a stochastic process near criticality, *Phys. Rev. X* **10**, 011032 (2020).
- [41] L. Marrec, I. Lamberti, and A.-F. Bitbol, Toward a Universal Model for Spatially Structured Populations, *Physical Review Letters* **127**, 218102 (2021).
- [42] A. Moawad, A. Abbara, and A.-F. Bitbol, Evolution of cooperation in deme-structured populations on graphs, *Physical Review E* **109**, 024307 (2024).
- [43] T. Maruyama, On the fixation probability of mutant genes in a subdivided population, *Genetics Research* **15**, 221 (1970).
- [44] N. Barton, The probability of fixation of a favoured allele in a subdivided population, *Genet. Res.* **62**, 149 (1993).
- [45] M. C. Whitlock and N. H. Barton, The effective size of a subdivided population, *Genetics* **146**, 427 (1997).
- [46] M. C. Whitlock, Fixation probability and time in subdivided populations, *Genetics* **164**, 767 (2003).
- [47] E. Lieberman, C. Hauert, and M. A. Nowak, Evolutionary dynamics on graphs, *Nature* **433**, 312 (2005).
- [48] B. Houchmandzadeh and M. Vallade, The fixation probability of a beneficial mutation in a geographically structured population, *New Journal of Physics* **13**, 073020 (2011).
- [49] B. Allen, G. Lippner, Y.-T. Chen, B. Fotouhi, N. Momeni, S.-T. Yau, and M. A. Nowak, Evolutionary dynamics on any population structure, *Nature* **544**, 227 (2017).
- [50] A. Abbara and A.-F. Bitbol, Frequent asymmetric migrations suppress natural selection in spatially structured populations, *PNAS Nexus* **2**, pgad392 (2023).
- [51] L. Marrec, Quantifying the impact of genotype-dependent gene flow on mutation fixation in subdivided

- populations, bioRxiv 10.1101/2023.11.29.569213 (2023).
- [52] S. Yagoobi and A. Traulsen, Fixation probabilities in network structured meta-populations, *Scientific Reports* **11**, 17979 (2021).
- [53] J. Tkadlec, K. Kaveh, K. Chatterjee, and M. A. Nowak, Evolutionary dynamics of mutants that modify population structure, *J. R. Soc. Interface* **20**, 20230355 (2023).
- [54] A. Abbara, L. Pagani, C. García-Pareja, and A.-F. Bitbol, Mutant fate in spatially structured populations on graphs: Connecting models to experiments, *PLOS Comput Biol* **20**, e1012424 (2024).
- [55] S. Kryazhimskiy, D. P. Rice, and M. M. Desai, Population subdivision and adaptation in asexual populations of *saccharomyces cerevisiae*, *Evolution* **66**, 1931 (2012).
- [56] J. R. Nahum, P. Godfrey-Smith, B. N. Harding, J. H. Marcus, J. Carlson-Stevermer, and B. Kerr, A tortoise-hare pattern seen in adapting structured and unstructured populations suggests a rugged fitness landscape in bacteria, *Proc Natl Acad Sci U S A* **112**, 7530 (2015).
- [57] P. P. Chakraborty, L. R. Nemzer, and R. Kassen, Experimental evidence that network topology can accelerate the spread of beneficial mutations, *Evolution Letters* **7**, 447 (2023).
- [58] J. Kreger, D. Brown, N. L. Komarova, D. Wodarz, and J. Pritchard, The role of migration in mutant dynamics in fragmented populations., *Journal of Evolutionary Biology* **36**, 444 (2023).
- [59] R. Lande, S. Engen, B.-E. Sæther, and B.-E. Saether, Extinction Times in Finite Metapopulation Models with Stochastic Local Dynamics, *Oikos* **83**, 383 (1998), 3546853.
- [60] C. Fruet, E. L. Müller, C. Loverdo, and A.-F. Bitbol, Spatial structure facilitates evolutionary rescue by drug resistance, *PLoS Comput Biol* **21**, e1012861 (2025).
- [61] S. Wright, Isolation by distance, *Genetics* **28**, 114 (1943).
- [62] S. Wright, Population Structure in Evolution, *Proceedings of the American Philosophical Society* **93**, 471 (1949), 3143336.
- [63] J. E. Keymer, P. Galajda, C. Muldoon, S. Park, and R. H. Austin, Bacterial metapopulations in nanofabricated landscapes, *Proceedings of the National Academy of Sciences* **103**, 17290 (2006).
- [64] P. Moran, *The Statistical Processes of Evolutionary Theory* (Oxford, UK: Clarendon, 1962).
- [65] R. Blythe and A. McKane, Stochastic models of evolution in genetics, ecology and linguistics, *J. Stat. Mech.* **P07018** (2007).
- [66] A. Traulsen and C. Hauert, Stochastic evolutionary game dynamics, *Reviews of Nonlinear Dynamics and Complexity* **2**, 25 (2009).
- [67] T. Antal and I. Scheuring, Fixation of strategies for an evolutionary game in finite populations, *Bulletin of Mathematical Biology* **68**, 1923 (2006).
- [68] I. Bena, Dichotomous Markov Noise: Exact results for out-of-equilibrium systems, *International Journal of Modern Physics B* **20**, 2825 (2006).
- [69] W. Horsthemke and R. Lefever, *Noise-Induced Transitions* (Springer, Berlin, 2006).
- [70] L. Ridolfi, P. D’Odorico, and F. Laio, *Noise-Induced Phenomena in the Environmental Sciences* (Cambridge University Press, Cambridge, U.K., 2011).
- [71] L. J. S. Allen, *An Introduction to Stochastic Processes with Applications to Biology*, 1st ed. (Pearson Education, 2003).
- [72] L. Witting, J. Seiffarth, B. Stute, T. Schulze, J. M. Hofer, K. Nöh, M. Eisenhut, A. P. M. Weber, E. von Lieres, and D. Kohlheyer, A microfluidic system for the cultivation of cyanobacteria with precise light intensity and CO<sub>2</sub> control: Enabling growth data acquisition at single-cell resolution, *Lab on a Chip* 10.1039/D4LC00567H (2024).
- [73] A. Rodriguez-Verdugo, C. Vulin, and M. Ackermann, The rate of environmental fluctuations shapes ecological dynamics in a two-species microbial system, *Ecology Letters* **22**, 838 (2019).
- [74] R. Hengge-Aronis, Survival of hunger and stress: The role of *rpoS* in early stationary phase gene regulation in *E. coli*, *Cell* **72**, 165 (1993).
- [75] C. R. Morley, J. A. Trofymow, D. C. Coleman, and C. Cambardella, Effects of freeze-thaw stress on bacterial populations in soil microcosms, *Microbial Ecology* **9**, 329 (1983).
- [76] F. Vasi, M. Travisano, and R. E. Lenski, Long-Term Experimental Evolution in *Escherichia coli*. II. Changes in Life-History Traits During Adaptation to a Seasonal Environment, *Am. Nat.* **144**, 432 (1994).
- [77] L. M. Wahl, P. J. Gerrish, and I. Saika-Voivod, Evaluating the Impact of Population Bottlenecks in Experimental Evolution, *Genetics* **162**, 961 (2002).
- [78] C. A. Fux, J. W. Costerton, P. S. Stewart, and P. Stoodley, Survival strategies of infectious biofilms, *Trends Microbiol.* **13**, 34 (2005).
- [79] M. Acar, J. T. Mettetal, and A. van Oudenaarden, Stochastic switching as a survival strategy in fluctuating environments, *Nat. Genet.* **40**, 471 (2008).
- [80] T. Proft, *Microbial Toxins: Current Research and Future Trends* (Caister Academic Press, 2009).
- [81] J. G. Caporaso, C. L. Lauber, E. K. Costello, D. Berg-Lyons, A. Gonzalez, J. Stombaugh, D. Knights, P. Gajer, J. Ravel, N. Fierer, J. I. Gordon, and R. Knight, Moving pictures of the human microbiome, *Genome Biol.* **12**, R50 (2011).
- [82] Y. Himeoka and N. Mitarai, Dynamics of bacterial populations under the feast-famine cycles, *Phys. Rev. Res.* **2**, 013372 (2020).
- [83] P. Tu, L. Chi, W. Bodnar, Z. Zhang, B. Gao, X. Bian, J. Stewart, R. Fry, and K. Lu, Gut microbiome toxicity: Connecting the environment and gut microbiome-associated diseases, *Toxics* **8**, 19 (2020).
- [84] M. H. A. Davis, Piecewise-Deterministic Markov Processes: A General Class of Non-Diffusion Stochastic Models, *Journal of the Royal Statistical Society. Series B (Methodological)* **46**, 353 (1984), 2345677.
- [85] P. Hufton, Y. T. Lin, T. Galla, and M. A. J, Intrinsic noise in systems with switching environments, *Phys. Rev. E* **93**, 052119 (2016).
- [86] M. J. Blaser and L. S. Newman, A Review of Human Salmonellosis: I. Infective Dose, *Reviews of Infectious Diseases* **4**, 1096 (1982).
- [87] M. H. Kothary and U. S. Babu, Infective Dose of Foodborne Pathogens in Volunteers: A Review, *Journal of Food Safety* **21**, 49 (2001).
- [88] M. Slatkin, Fixation probabilities and fixation times in a subdivided population, *Evol.* **35**, 477 (1981).
- [89] P. L. Krapivsky, S. Redner, and E. Ben-Naim, *A Kinetic View of Statistical Physics* (Cambridge University Press, Cambridge, USA, 2010).
- [90] U. C. Täuber, *Critical Dynamics* (Cambridge University Press, Cambridge, USA, 2014).

- [91] K. Totlani, J.-W. Hurkmans, W. M. van Gulik, M. T. Kreutzer, and V. van Steijn, Scalable microfluidic droplet on-demand generator for non-steady operation of droplet-based assays, *Lab Chip* **20**, 1398 (2020).
- [92] R. H. Hsu, R. L. Clark, J. W. Tan, J. C. Ahn, S. Gupta, P. A. Romero, and O. S. Venturelli, Microbial interaction network inference in microfluidic droplets, *Cell Syst.* **9**, 229 (2019).
- [93] S. Ganchua, A. White, E. Klein, and J. Flynn, Lymph nodes – the neglected battlefield in tuberculosis, *PLoS Pathogens* **16**, e1008632 (2020).
- [94] W. Van den Broeck, A. Derore, and P. Simoens, Anatomy and nomenclature of murine lymph nodes: Descriptive study and nomenclatory standardization in balb/cannrl mice, *Journal of immunological methods* **312**, 12 (2020).
- [95] G. Lambert and E. Kussell, Memory and fitness optimization of bacteria under fluctuating environments, *PLoS Genet.* **10**, e1004556 (2014).
- [96] F. Abdul-Rahman, D. Tranchina, and D. Gresham, Fluctuating environments maintain genetic diversity through neutral fitness effects and balancing selection, *Mol. Biol. Evol.* **38**, 4362 (2021).
- [97] M. Asker, M. Swailem, U. C. Täuber, and M. Mobilia, Supporting data and codes, *Research Data Leeds Repository*, (<https://doi.org/TBC>) (2025).
- [98] D. T. Gillespie, A general method for numerically simulating the stochastic time evolution of coupled chemical reactions, *J. Comput. Phys.* **202**, 403 (1976).